Catalysis Today 183 (2012) 154–171

Contents lists available at SciVerse ScienceDirect

Catalysis Today

journal homepage: www.elsevier.com/locate/cattod

Colloidal Ru, Co and Fe-nanoparticles. Synthesis and application as nanocatalysts in the Fischer–Tropsch process

Aitor Gual[a], Cyril Godard[b], Sergio Castillón[c], Daniel Curulla-Ferré[d], Carmen Claver[b,*]

[a] Centre Tecnòlogic de la Química de Catalunya, C/Marcel.li Domingo s/n, 43007 Tarragona, Spain
[b] Departament de Química Física I Inorgànica, Universitat Rovira I Virgili, C/Marcel.li Domingo s/n, 43007 Tarragona, Spain
[c] Departament de Química Analítica I Orgànica, Universitat Rovira I Virgili, C/Marcel.li Domingo s/n, 43007 Tarragona, Spain
[d] Gaz & Energies Nouvelles, Total S.A. Paris La Defense 6, France

ARTICLE INFO

Article history:
Received 25 September 2011
Received in revised form
17 November 2011
Accepted 18 November 2011
Available online 18 December 2011

Keywords:
Soluble nanoparticles
Preparation of nanoparticles
Stabilising agents
Ru, Co, Fe
Catalysis
Fischer–Tropsch

ABSTRACT

In this review, the current state of the art in the synthesis of soluble-Ru, Co and Fe-nanoparticles stabilised by organic molecules is described. Polymers are widely applied for the synthesis of soluble-Ru, Co and Fe-NPs, whereas the application of surfactants, ionic liquids and small molecules is much more limited.

The recent applications of soluble-metal NPs as catalysts in the Fischer–Tropsch synthesis are described. The application of soluble-metal nanocatalysts in the Fischer–Tropsch reaction using water, ionic liquids and high boiling point organic solvents is reviewed showing that higher activities and selectivities than those obtained using conventional supported catalysts can be achieved.

1. Introduction

An ever-increasing interest is devoted to chemical species of nanometric size [1–11]. Metal nanoparticles (M-NPs) are in this respect of special interest, due to their many properties which may be exploited [12]. M-NPs display optical, magnetic, electronic and catalytic properties and are currently applied in catalysis and other chemical processes, biology, microelectronics or nanoelectronics.

Since the properties of the M-NPs are in general size dependant, it is essential to control their size in order to reach a monodisperse assembly of particles exhibiting the desired features [1–11]. In addition, it is important to control their organization to be able to address the particles in selected devices. Furthermore, a large proportion of the atoms present in a NP are situated at the surface and therefore, the chemical and physical properties of the NPs will be strongly influenced by the nature of the surface species. In this context, the method used for the synthesis of the M-NPs and the nature of the stabilising agents are of critical importance and will be described in this review.

Catalysis is one of the most important application of M-NPs [1–11,13]. As catalysts, these systems show a great potential because of the high ratio of atoms remaining at the surface, and which are therefore available for acting in the chemical transformation of the substrates. The recovery of the M-NPs catalysts are currently carried out by three approaches: (a) colloidal M-NPs in a biphasic media, (b) nanofiltration and (c) supported M-NPs. Concerning colloidal M-NPs, stabilizating agents such as polymers, ionic surfactants, ionic liquids and small molecules containing coordinating atoms are currently utilised as protective agents to prevent the M-NPs aggregation and/or to facilitate catalysts recycling.

Concerning the Fischer–Tropsch reaction (Scheme 1a), the most active metals are ruthenium followed by iron, nickel, and cobalt and in terms of selectivity, the molecular average weight of the produced hydrocarbons decreased in the following sequence: Ru > Fe > Co > Rh > Ni > Ir > Pt > Pd [14]. Ru and Rh are too expensive and Ni catalysts produce too much methane under practical conditions. Thus, only Fe and Co display appropriate catalytic characteristics for industrial application. However, some examples of Ru were reported at laboratory scale. Although at low conversions, the activities of Fe and Co are comparable, the productivity at higher conversion is superior using Co-based catalysts. Concerning their selectivity, both metals (Fe and Co) display similar chain growth cabalities at relatively low temperatures (ca. 473–523 K)

* Corresponding author. Fax: +34 977 559563.
E-mail address: carmen.claver@urv.cat (C. Claver).

0920-5861/$ – see front matter © 2011 Published by Elsevier B.V.
doi:10.1016/j.cattod.2011.11.025

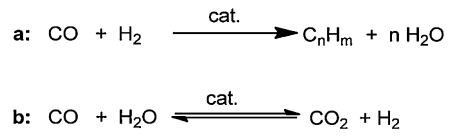

Scheme 1. Fischer–Tropsch synthesis and water gas shift equilibrium.

[15]. Water generated by the Fischer–Tropsch synthesis slows the reaction rate on Fe to a greater extent than on Co catalysts, and the water–gas shift reaction is more significant on Fe than on Co catalysts (Scheme 1b).

In this review, the different synthetic methods to obtain colloidal Ru^0, Co^0 and Fe^0-NPs are described and their catalytic applications in Fischer–Tropsch processes are presented.

2. Synthetic methods for the preparation of colloidal metal nanoparticles

The methods used to synthesise M-NPs are commonly classified as "top-down" and "bottom-up" approaches (Scheme 2). The top-down approach is subject to drastic limitations for dimensions smaller than 100 nm. This size restriction and the high cost of this approach make the bottom-up approach the most promising strategy. The bottom-up approach approximation consists in the synthesis of M-NPs starting from metallic molecules by "stabilisation of M-NPs procedures" [16].

Generally, M-NPs are unstable with respect to agglomeration towards the bulk since at short interparticle distances and in the absence of any repulsive effect, the van der Waals forces will attract two M-NPs to each other favouring their agglomeration [7,13,17,18]. Hence, it is necessary to use capping agents to provide stable M-NPs in solution. Nanocluster stabilisation is usually discussed in terms of two general categories: (i) electrostatic stabilisation and (ii) steric stabilisation.

Ionic compounds such as halides, carboxylates, or polyoxoanions, in solution (generally aqueous) can perform electrostatic stabilisation of M-NPs [7,13,17,18]. The presence of these compounds and their related counter-ions surrounding the metallic surface will generate an electrical double-layer around the M-NPs (Fig. 1, left). This results in a Coulombic repulsion between the M-NPs. If the electric potential associated with the double layer is high enough, then the electrostatic repulsion will prevent particle aggregation. Colloidal M-NPs stabilised by electrostatic repulsion are very sensitive to any change in the medium that enables to disrupt the double layer.

In the case of steric stabilisation, organic molecules which present coordinating groups in its molecular structure can prevent M-NPs aggregation by providing a protective layer (Fig. 1, right) [7,13,17,18]. In contrast with the electrostatic stabilisation, which is mainly used in aqueous media, the steric stabilisation can be used in organic or in aqueous phase. Nevertheless, the length and/or the nature of the macromolecules used influence the thickness of the protective layer and can thus modify the stability of the colloidal M-NPs. It has been reported that M-NPs can also be stabilised by the sole effect of the coordinating solvent molecules [19,20]. However, it has not been entirely established if other stabilising agents such as anions or cations involved in the synthesis of the M-NPs could also contribute to their stabilisation [21].

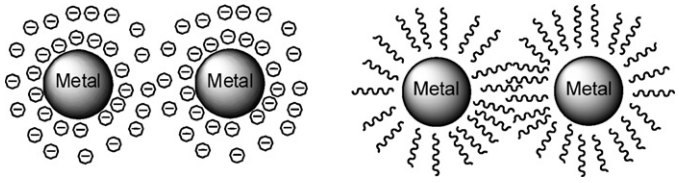

Fig. 1. Schematic representation of the electrostatic (left) and steric (right) stabilisation of M-NPs.

Finally, the electrostatic and steric stabilisation can be combined to maintain M-NPs stable in solution [7,13]. This type of stabilisation is generally provided by ionic surfactants, which contain a polar group able to generate an electronic double layer and a lipophylic side chain able to provide steric repulsion.

An important variable in the synthesis of M-NPs is the use of methods that allow control over the particle size and composition [7,13]. Furthermore, the synthetic approach has to produce isolable and re-dissolvable M-NPs and it has to be reproducible. Chemical methods provided a reproducible synthesis of M-NPs with small size and narrow dispersion, and they are preferred to the physical methods (Scheme 2). The selected chemical method to synthesise M-NPs essentially depends on the metal oxidation state of the molecular precursor [7,13]. If the metal centre in the precursor displayed high oxidation states (M^{n+}), strong reducing agents are required to obtain the desired M-NPs. This reducing agent can be the solvent, the stabiliser, a reducing gas such as CO or H_2 (Scheme 3a), hydrides such as $NaBH_4$ (Scheme 3b) or other reducing agents.

The organometallic approach to synthesise M-NPs through ligand displacement was developed by Chaudret and co-workers [7,10,11,13]. The advantage of this methodology is the possibility to obtain M-NPs with clean surfaces by decomposition of organometallic precursors, usually low valence state organometallic complexes, under mild conditions. Furthermore, this methodology also offers the possibility to stabilise M-NPs with a high degree of control on the size, shape and surface environment.

Organometallic precursors can be decomposed by ligand deplacement using H_2 as a reducing gas (Scheme 4) [11]. The ideal precursors are zerovalent olefinic metal complexes, such as [Ru(COD)(COT)] (COD: 1,5-cyclooctadiene, COT: 1,3,5-cyclooctatetraene). However, these procedures can also be carried out by decomposition of organometallic complexes which contain other types of ligands that can be displaced by hydrogenolysis. For instance, precursors such as $[Rh(\eta^3\text{-}C_3H_5)_3]$, $[Co(\eta^3\text{-}C_8H_{13})(\eta^4\text{-}C_8H_{12})]$, $[Rh(\mu\text{-}OMe)(COD)]_2$, $Co[N(SiMe_3)_2]_2$ and $Fe[N(SiMe_3)_2]_2$ were successfully utilised [11]. M-NPs were also synthesised by decomposition of zerovalent carbonylic complexes, such as $[Ru_3(CO)_{12}]$, $[Co_2(CO)_8]$ and $[Fe(CO)_5]$ [22,23].

3. Stabilisers used for the synthesis of colloidal Ru-nanoparticles

3.1. Polymers

The stabilisation of metal-NPs by polymers, and in particular polyvinylpyrrolidone (PVP), has been largely described since this stabilising agent is non-toxic and soluble in many polar solvents [24]. These polymers are characterized by their molecular weight, which is referred to as PVP K-*n* (*n* = 15, 30 or 90) in this review (Fig. 2).

Chain-like Ru-NPs arrays of 1.0–3.0 nm in diameter and ~280 nm in length were synthesised by H_2 reduction (ca. 10 bar) of $RuCl_3$ in presence of PVP (K-15, K-30 and K-90) at 80 °C in aqueous media (entries 1–3, Table 1) [25,26].

The morphology of these Ru-NPs could be varied from long chain-like to cross-linked arrays by adjusting some of the reaction conditions such as the average molecular weight of PVP and the molar ratio of PVP monomer to Ru. These M-NPs were described as microreactors in the aqueous/organic hydrogenation of arenes, since in this system PVP provides a hydrophobic microenvironment that prevents the nanoparticles from aggregation in water.

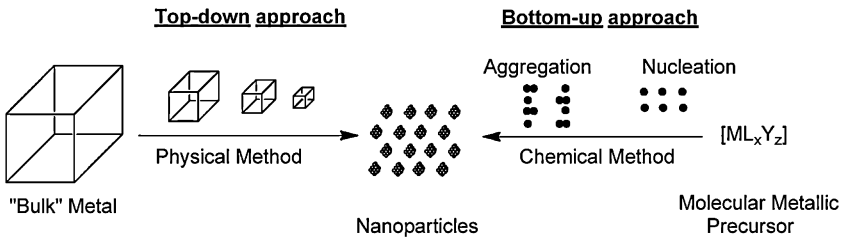

Scheme 2. Schematic representation of the preparative methods for the synthesis of M-NPs.

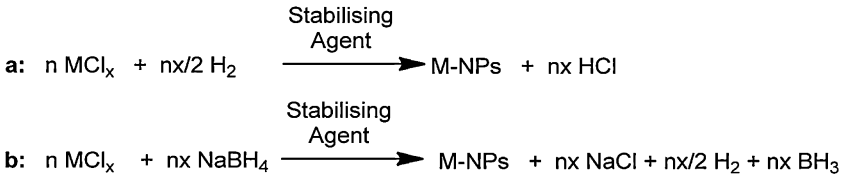

Scheme 3. Synthesis of M-NPs by reduction of MCl_x precursor (a) using H_2 as the reducing agent, and (b) using $NaBH_4$ as the reducing agent.

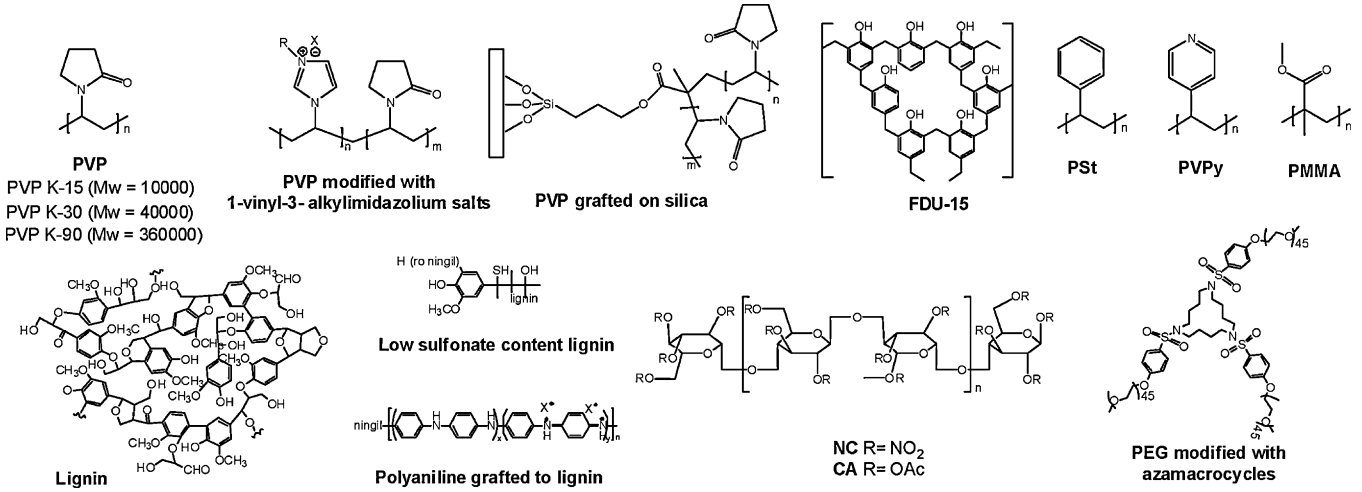

Fig. 2. Polymers used as stabilising agents in the synthesis of Ru-NPs.

The high activity of these Ru-NPs catalysts for the hydrogenation of arenes was explained by the fact that catalyst and substrates are confined in the hydrophobic pocket formed by the microreactor, which enhances the contact between them. With this protocol, fast aqueous/organic hydrogenation of arenes, olefins and carbonyl compounds can be achieved using this Ru/PVP-NPs microreactor system [25,26].

Kou and co-workers reported the synthesis of water-soluble Ru-NPs stabilised by PVP K-30 by reduction of $RuCl_3$ (entries 4–5, Table 1) and studied the effect of the PVP K-30/Ru ratio (20, 40 and 200) and the reduction method: (a) 20 bar H_2 at 150 °C, and (b) addition of $NaBH_4$ at room temperature [27]. They observed that the M-NPs diameter is mainly affected by the PVP K-30/Ru ratio, 2.0 nm and 1.8 nm for PVP/Ru ratio of 40 and 200, respectively.

Table 1
Ru-NPs synthesised by reduction of $RuCl_3$ in presence of polymers.

Entry	Stabilising agent	Reducing agent	Solvent	Ru-NPs size	Ref.
1	PVP K-15	H_2 (10 bar) at 80 °C	H_2O	1–3 nm	[25,26]
2	PVP K-30	H_2 (10 bar) at 80 °C	H_2O	1–3 nm	[25,26]
3	PVP K-90	H_2 (10 bar) at 80 °C	H_2O	1–3 nm	[25,26]
4	PVP K-30	H_2 (20 bar) at 150 °C	H_2O	1.8–2.0 nm	[27]
5	PVP K-30	$NaBH_4$ addition at r.t.	H_2O	1.8–2.0 nm	[27]
6	PVP K-30	H_2 (20 bar) at 150 °C	H_2O	1.9 nm	[28]
7	PVP K-30	$NaBH_4$ addition at r.t.	H_2O	2.2 nm	[28]
8	PVP K-30	N_2H_4 addition at r.t.	H_2O	1.8 nm	[28]
9	Low sulfonate content lignin	H_2 (20 bar) at 150 °C	H_2O	1.9 nm	[28]
10	Polyaniline grafted to lignin	H_2 (20 bar) at 150 °C	H_2O	3–6 nm	[28]
11	PVP K-30	Ethyleneglycol (EG)	EG	1–6 nm	[29]
12	PVP K-30	Photoreduction	H_2O/EtOH	1.3 nm	[31]
13	FDU-15	H_2 flow at 350 °C or HCOONa at 100 °C	H_2O	1.7–1.8 nm	[32]
14	Polystyrene (PSt)	$NaBH_4$ addition at r.t.	H_2O	16.0 nm	[33]
15	Poly(4-vinyl-pyridine) (PVPy)	$NaBH_4$ addition at r.t.	H_2O	1–2 nm	[34]

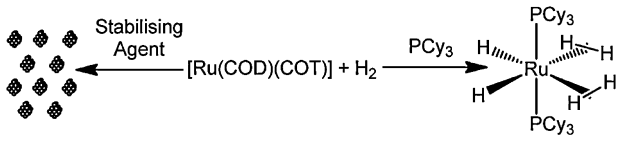

Scheme 4. Synthesis of Ru-NPs versus molecular complex by decomposition of [Ru(COD)(COT)] precursor through ligand displacement and reduction with dihydrogen.

Interestingly, the Ru-NPs synthesised using H_2 as reducing agent provided much higher activity in the aqueous-phase Fischer–Tropsch synthesis than those synthesised using $NaBH_4$. Furthermore, they reported also the synthesis of Ru-NPs stabilised by PVP modified with imidazolium salts (Fig. 2) and their application as nanocatalysts in the Fischer–Tropsch process [27]. However, lower activities than those obtained with the Ru/PVP K-30-NPs were obtained.

Recently, our research group studied the effect on the Ru-NPs mean diameter and size distribution of the stabilising agent (PVP vs. lignins) and the reduction method: (a) 3–20 bar H_2 at 60–150 °C, (b) addition of $NaBH_4$ at room temperature, and (c) addition of N_2H_4 at room temperature (entries 6–10, Table 1) [28]. Using a PVP/Ru ratio of 20, N_2H_4 (ca. 1.8 nm) reduction of $RuCl_3$ produced smaller Ru-NPs than with H_2 (ca. 1.9 nm) and $NaBH_4$ (ca. 2.2 nm) (entries 6–8, Table 1). Using H_2 as reducing agent, no significant effect on the mean diameter of the Ru-NPs was observed by varying the hydrogen pressure (ca. 3, 10 and 20 bar) and the reaction temperature (60, 120 and 150 °C). As previously mentioned, the use of higher PVP/Ru ratio (ca. 200) produces smaller Ru-NPs (1.6–1.7 nm). Commercially available low-sulfonate content lignin (Fig. 2) stabilised Ru-NPs of similar mean diameters and size distributions than those obtained using PVP K-30, whereas larger Ru-NPs (ca. 3–6 nm) were obtained using polyaniline grafted to lignin (Fig. 2) as stabilising agent (entries 9–10, Table 1).

Ru-NPs stabilised by PVP K-30 were synthesised by reduction of $RuCl_3$ in polyols (ethylene glycol, diethylene glycol and triethylene glycol) [29]. The polyol acts as a solvent, reducing agent and stabilising agent [30]. Using this methodology, it is possible to control the growing of the NPs in order to obtain a wide range of Ru-NPs sizes (ca. 1–6 nm) (entry 11, Table 1) [29]. Ru-NPs of 1.3 nm were synthesised by photoreduction of $RuCl_3$ promoted by ketyl radicals in presence of PVP K-30 (entry 12, Table 1) [31].

Ru-NPs of 1.7–1.8 nm stabilised by the polyphenol FDU-15 (Fig. 2) were synthesised by reduction of $RuCl_3$ in presence of a H_2 flow at 350 °C or by addition of HCOONa at 100 °C (entry 13, Table 1) [32]. The Ru/FDU-15-NPs catalysts are active in the hydrogenation of arenes providing comparable TOFs to those obtained with the Ru/PVP-K90-NPs. Ru-NPs of 16.0 nm were obtained by chemical reduction of $RuCl_3$ using $NaBH_4$ as reducing agent and monodisperse polystyrene (PSt) (Fig. 2) microspheres as stabilisers (entry 14, Table 1) [33]. These NPs were applied as nanocatalyst in the generation of H_2 from alkaline solution of $NaBH_4$. Ru-NPs of 1–2 nm were synthesised by $NaBH_4$ reduction of $RuCl_3$ in presence of poly(4-vinyl-pyridine) (PVPy) (Fig. 2) as the stabiliser (entry 15, Table 1) [34]. These nanocatalysts were applied in the hydrogenation of quinoline.

The synthesis of γ-alumina supported Ru/PVP K-30-NPs was reported by: (a) immobilization of the PVP-stabilised Ru-NPs onto the support, or (b) in situ deposition of Ru-NPs, e.g., reduction of $RuCl_3$ with ethyleneglycol (EG) in the presence of the γ-alumina [29a]. Ru-NPs were also synthesised by alcohol reduction of $RuCl_3$ in presence of PVP/β-zeolite [35]. These NPs are effective catalysts in the hydrogenation of benzene. Ru-hydroxyl-terminated poly(amidoamine) (PAMAM-OH)/Al_2O_3 catalysts were synthesised by chemical reduction of $RuCl_3$ through H_2 treatment at 300 °C [36].

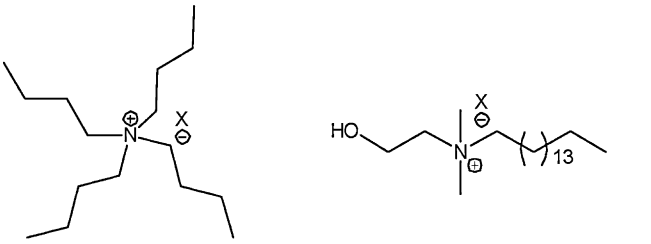

Fig. 3. Surfactants used as stabilising agents in the synthesis of Ru-NPs.

This approach produced Ru-NPs with a narrow particle size distribution. Recently, the synthesis of PVP chemically grafted onto silica and their application in the stabilisation of Ru-NPs was described [37]. The Ru-NPs were synthesised by chemical reduction of $RuCl_3$ at room temperature using $NaBH_4$ as reducing agent in presence of PVP on silica. The size distribution of the Ru-NPs was 2.0–5.0 nm. These Ru-NPs exhibit excellent catalytic activity for the hydrogenation of arenes [37].

Polymers can also be used in the synthesis of Ru-NPs by ligand reduction and displacement from organometallic precursors. $[Ru(C_8H_{12})(C_8H_{10})]$ reacts rapidly with H_2 (ca. 1–3 bar) at room temperature in an organic solvent to give Ru-NPs and cyclooctane (Table 2) [38–43]. Using this methodoly, Ru-NPs were obtained in the presence of polymers, such as PVP K-30, nitrocellulose (NC) or cellulose acetate (CA) (Fig. 2). The Ru-NPs mean diameters and size distributions depend on the nature of the polymer and the metallic precursor–polymer ratio [38–41]. Using this method, small Ru-NPs were prepared in PVP K-30 (ca. 1.1 nm) and NC (ca. 1.3 nm) (entries 1–2, Table 2). In both cases, the Ru-NPs displayed very low size dispersity. In contrast, the reaction in CA produced larger Ru-NPs (1.7 nm) displaying a broader size dispersity, which evidences the influence of the nature of the polymer and of its coordination ability on the stabilisation of the Ru-NPs (entry 3, Table 2). Water soluble Ru-NPs of 1.9 nm were synthesised by decomposition of $[Ru(C_8H_{12})(C_8H_{10})]$ with 3 bar H_2 at room temperature using polyethyleneglycol modified (mod-PEG) with azamacrocycles (Fig. 2) as stabiliser (entry 4, Table 2) [42]. Ru-NPs of 2.5 nm and 1.9 nm were obtained by solid-state decomposition of $[Ru(C_8H_{12})(C_8H_{10})]$ in presence of a polymer as stabilising agent such as polystyrene (PSt) and poly(methylmethacrylate) (PMMA) (Fig. 2), respectively (entries 5–6, Table 2) [43].

3.2. Ionic surfactants

A typical approach to stabilise M-NPs in the aqueous phase and to prevent their aggregation is the use of surfactants, such as tetraalkylammonium salts. In 1997, water-soluble Ru-NPs were stabilised by tetrabutylammonium (TBA) salts (Fig. 3) by reduction of $RuCl_3$ using H_2 as reducing agent [44]. These NPs were successfully applied in the hydrogenation of 2-methoxy-4-propylphenol under a biphasic medium.

More recently, the use of ionic surfactants as stabilising agents for the synthesis of water-soluble M-NPs and their application as catalysts in arene hydrogenation in pure biphasic liquid–liquid (water/substrate) media at room temperature was intensively studied [45]. In the case of Ru, small NPs (2.5–3.5 nm) were synthesised by chemical reduction of $RuCl_3$ using $NaBH_4$ as reducing agent and 2 equiv. of N,N-dimethyl-N-cetyl-N-(2-hydroxyethyl) ammonium chloride salt (HEA-16-Cl) as stabiliser (Fig. 3) [45e]. These Ru/HEA-16-Cl-NPs were shown to be active in the hydrogenation of various aromatic compounds with moderate to high activities. Furthermore, water-soluble Ru-NPs stabilised by mixtures of

Table 2
Ru-NPs synthesised by decomposition of $[Ru(C_8H_{12})(C_8H_{10})]$ in presence of polymers and 1–3 bar H_2.

Entry	Stabilising agent	Solvent	Ru-NPs size	Ref.
1	PVP K-30	THF	1.1 nm	[38–41]
2	Nitrocellulose (NC)	THF	1.3 nm	[38–40]
3	Cellulose acetate (CA)	THF	1.7 nm	[38–40]
4	Polyethyleneglycol modified (mod-PEG) with azamacrocycles	THF	1.9 nm	[42]
5	Polystyrene (PSt)	–	2.5 nm	[43]
6	Poly(methylmethacrylate) (PMMA)	–	1.9 nm	[43]

HEA-16-Cl and cyclodextrins (CD) were obtained by reduction of $RuCl_3$ using $NaBH_4$ as reducing agent [46]. These particles are monodisperse in size with an average diameter of about 4.0 nm. Interestingly, these Ru-NPs were found to be more active in the hydrogenation of arenes than those stabilised only by HEA-16-Cl. These results were explained by the possible interaction of the CD with the surfactant at the surface and the organic substrate [46].

3.3. Ionic liquids

M-NPs are obtained by simple reduction of transition-metal compounds dissolved in imidazolium ionic liquids (IL) in the presence of molecular hydrogen (Fig. 4) [47]. The size of "soluble" metal nanoparticles is directly related to the ionic liquid self-organization and thus can be tuned by modulating the reaction temperature, length of the N-alkyl imidazolium side chains or anion volume [48]. M-NPs in imidazolium ILs are stabilised by protective layers of discrete supramolecular species $\{[(DAI)_x(X)_{x-n}]^{n+}[(DAI)_{x-n}(X)_x]^{n-}\}_n$ (DAI = dialkylimidazolium cation and X anion) through interactions of anionic moieties and N-heterocycle carbenes [49]. These weakly surface-bound protective species could be easily displaced by other substances present in the media affecting their catalytic activity and stability against aggregation and/or oxidation [50].

Concerning the Ru-NPs, their synthesis was performed using different metallic precursors ($[Ru(C_8H_{12})(C_8H_{10})]$, $[Ru(C_8H_{12})(2\text{-methylallyl})_2]$, RuO_2) using H_2 (ca. 4 bar H_2) as reducing agent at 75 °C and several different imidazolium cations (1-*n*-butyl-3-methylimidazolium [BMI], 1-*n*-decyl-3-methylimidazolium [DMI], and 1-butyronitrile-3-methylimidazolium [(BCN)MI]) and anions (PF_6-NTf_2-BF_4) as stabilising agents (entries 1–11, Table 3) [50–53]. These Ru-NPs are monodisperse in size with an average diameter of 2.0–3.0 nm and they are efficient catalysts in the hydrogenation of arenes. These Ru-NPs can be used in biphasic, homogeneous and heterogeneous hydrogenation of arenes and they were active under mild reaction conditions. Interestingly, the reactions performed under solventless (heterogeneous) conditions were found to be faster than those performed with the NPs dispersed in IL (biphasic system), which was explained by the influence of mass-transfer-processes typical of a multiphase system. As an alternative procedure, Ru-NPs of 1.6, 2.0 and 1.6 nm were synthesised by decomposition of $[Ru_3(CO)_{12}]$ in presence of $[BMI{\cdot}BF_4]$ using microwave irradiation, photocatalytic treatment and thermal treatment at 155 °C (entries 12–14, Table 3) [54].

Other types of ionic liquids, 1,1,3,3-tetra-methylguanidinium (TMG) and tri-hexyl-tetradecylphosphonium (THTdP) salts (Fig. 4), were also applied as stabilising agents for the synthesis of Ru-NPs [55–57]. Ru-NPs of 2.0–5.0 nm and 1.2 nm were synthesised by H_2 reduction (ca. 10–30 bar) of $RuCl_3$ at 150–220 °C in presence of a mixture of 1,1,3,3-tetramethylguanidinium lactate (TMGL)-SBA-15 and 1,1,3,3-tetramethylguanidinium trifluoroacetate ([TMG][TFA])-montmorillonite (MMT) [55,56]. Recently, Zeng and co-workers described the synthesis of highly dispersed PtRu-NPs on composite film of multi-walled carbon nanotubes (MWNTs)–IL trihexyltetradecylphosphonium bis(trifluoromethyl sulfonyl) imide ($THTdP{\cdot}NTf_2$) using ultrasonic-electrodeposition method [57].

3.4. Small molecules

Small molecules, in general used as ligands in coordination chemistry, containing donor atoms in their structure can also be effectively used as stabilising agents for the synthesis of Ru-NPs. Generally, the synthesis was carried by decomposition (3 bar H_2 at room temperature) of $[Ru(C_8H_{12})(C_8H_{10})]$ in presence substoichiometric quantities of this type of molecules [11].

It was demonstrated that thiols (2.0–3.0 nm), amines (2.0–3.0 nm), alcohols (3.0 nm), silanes (2.3 nm) and phosphorus donor compounds (1.3–4.0 nm) were able to stabilise Ru-NPs [11,58–61]. These Ru-NPs catalysed the hydrogenation of arenes under milder reaction conditions than the classical heterogeneous catalysts and in several cases higher levels of selectivity were achieved [58].

4. Stabilisers used for the synthesis of colloidal Co-nanoparticles

4.1. Polymers

Co-NPs of 7.2 ± 2.1 nm stabilised by PVP K-30 (Fig. 5) were prepared by $NaBH_4$ reduction of $CoCl_2{\cdot}6H_2O$ in methanol solution at 80 °C (entry 1, Table 4) [62]. These Co-NPs were soluble in water and they were applied as catalysts in the hydrogen generation from the hydrolysis of ammonia-borane and $NaBH_4$. Kou and co-workers reported the synthesis of water-soluble Co-NPs stabilised by PVP K-30 using KBH_4 as reducing agent and their application as nanocatalysts in the Fischer–Tropsch process (entry 2, Table 4) [63]. Kou and co-workers also described the synthesis Co-NPs of size range 15–30 nm by thermal decomposition of $[Co_2(CO)_8]$ using squalene and toluene as a solvents and PVP-C8 (Fig. 5) as stabilising agent (entry 3, Table 4) [64]. This Co-NPs were successfully tested in the Fischer–Tropsch reaction. Recently, we were focussed in the synthesis of Co-NPs stabilised by PVP K-30. We studied the effect of the PVP K-30/Co ratio (20, 40 and 200) and the synthetic methodology: (a) reduction of metallic salts, and (b) thermal decomposition of $[Co_2(CO)_8]$ [28]. We observed that the PVP K-30/Co ratio as well as the synthetic methodology highly affected the mean diameter and size dispersion of the produced Co-NPs (ca. 2–5 nm) (entries 4–5, Table 4).

The synthesis of water-soluble Co-NPs stabilised by alkyl thioether end-functionalized poly(methacrylic acid) (PMAcDDT) was carried out by reduction $CoCl_2{\cdot}6H_2O$ using $NaBH_4$ as reducing agent (entry 6, Table 4) [65]. The authors observed that the size of the spherical nanoparticles could be tuned between 2 and 7.5 nm by changing the concentration of the polymer.

Water-soluble Co-NPs of 3.5 ± 1.0 nm stabilised by the perfluorinated sulfo-cation membrane (MF-4SK) were synthesised by reduction of $CoCl_2{\cdot}6H_2O$ using $NaBH_4$ as reducing agent (entry 7, Table 4) [66]. The synthesis of Co-NPs of 5.3–6.3 nm stabilised by microcrystalline cellulose (MCC) (Fig. 5) matrix was carried out by

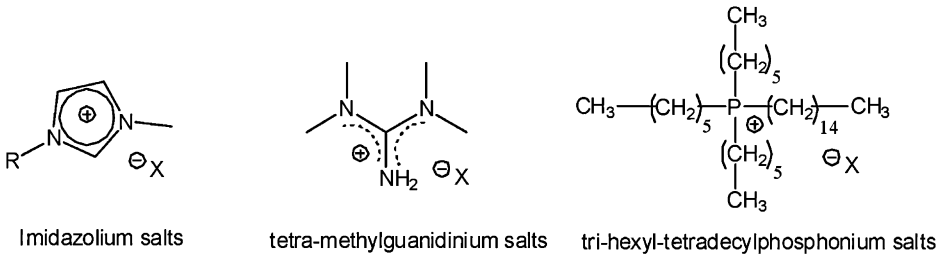

Fig. 4. Ionic liquids used as stabilising agents in the synthesis of Ru-NPs.

Table 3
Ru-NPs stabilised by imidazolium ionic liquids.

Entry	Metallic precursor	Stabilising agent	Synthetic procedure	Ru-NPs size	Ref.
1	$[Ru(C_8H_{12})(C_8H_{10})]$	1-*n*-Butyl-3-methylimidazolium hexafluorophosphate [BMI·PF_6]	H_2 (4 bar) at 75 °C	2.6 nm	[50]
2	$[Ru(C_8H_{12})(C_8H_{10})]$	1-*n*-Butyl-3-methylimidazolium tetrafluoroborate [BMI·BF_4]	H_2 (4 bar) at 75 °C	2.6 nm	[50]
3	$[Ru(C_8H_{12})(C_8H_{10})]$	1-*n*-Butyl-3-methylimidazolium trifluoromethane sulfonate [BMI·CF_3SO_3]	H_2 (4 bar) at 75 °C	2.6 nm	[50]
4	$[Ru(C_8H_{12})(C_8H_{10})]$	1-*n*-Butyl-3-methylimidazolium N-bis(trifluo romethanesulfonyl)imidate [BMI·NTf_2]	H_2 (4 bar) at 50 °C	2.6 nm	[51]
4	$[Ru(C_8H_{12})(2\text{-methylallyl})_2]$	1-*n*-Butyl-3-methylimidazolium N-bis(trifluo romethanesulfonyl)imidate [BMI·NTf_2]	H_2 (4 bar) at 50 °C	2.1 nm	[52a]
5	$[Ru(C_8H_{12})(2\text{-methylallyl})_2]$	1-*n*-Butyl-3-methylimidazolium tetrafluoroborate [BMI·BF_4]	H_2 (4 bar) at 50 °C	2.9 nm	[52a]
6	$[Ru(C_8H_{12})(2\text{-methylallyl})_2]$	1-*n*-Decyl-3-methylimidazolium N-bis(trifluoro methanesulfonyl)imidate [DMI·NTf_2]	H_2 (4 bar) at 50 °C	2.1 nm	[52a]
7	$[Ru(C_8H_{12})(2\text{-methylallyl})_2]$	1-*n*-Butyl-3-methylimidazolium tetrafluoroborate [BMI·BF_4]	H_2 (4 bar) at 50 °C	2.7 nm	[52a]
8	$[Ru(C_8H_{12})(2\text{-methylallyl})_2]$	1-Butyronitrile-3-methylimidazolium-bis(tri-fluoromethane-sulfonyl)-imidate [(BCN)MI·NTf_2]	H_2 (4 bar) at 50 °C	2.2 nm	[52b]
9	$RuO_2{\cdot}3H_2O$	1-*n*-Butyl-3-methylimidazolium hexafluorophosphate [BMI·PF_6]	H_2 (4 bar) at 75 °C	2.6 nm	[53]
10	$RuO_2{\cdot}3H_2O$	1-*n*-Butyl-3-methylimidazolium tetrafluoroborate [BMI·BF_4]	H_2 (4 bar) at 75 °C	2.6 nm	[53]
11	$RuO_2{\cdot}3H_2O$	1-*n*-Butyl-3-methylimidazolium trifluoromethanesulfonate [BMI·CF_3SO_3]	H_2 (4 bar) at 75 °C	2.6 nm	[53]
12	$[Ru_3(CO)_{12}]$	1-*n*-Butyl-3-methylimidazolium tetrafluoroborate [BMI·BF_4]	Microwave irradiation	1.6 nm	[54]
13	$[Ru_3(CO)_{12}]$	1-*n*-Butyl-3-methylimidazolium tetrafluoroborate [BMI·BF_4]	Photocatalytic decomposition	2.0 nm	[54]
14	$[Ru_3(CO)_{12}]$	1-*n*-Butyl-3-methylimidazolium tetrafluoroborate [BMI·BF_4]	Thermal decomposition at 155 °C	1.6 nm	[54]

reduction of $Co(AcO)_2{\cdot}4H_2O$ and $CoSO_4{\cdot}7H_2O$ using NaH_2PO_2 as reducing agents (entry 8, Table 4) [67].

Co-NPs of 7 ± 1 nm were synthesised by thermal decomposition of $[Co_2(CO)_8]$ in presence of thermo-responsive polymers (entry 9, Table 4) [68]. These polymers are based on poly(N-isopropyl-co-*t*-butylacrylamide) (Fig. 5), synthesised to contain a thioether terminated with a carboxylic acid for interaction with NPs surfaces. The as-prepared Co-NPs were water soluble below 25 °C due to the conformational change of the polymer from hydrophobic (at high temperature) to hydrophilic (at lower temperature). Co-NPs were also synthesised by thermal decomposition of $[Co_2(CO)_8]$ in the presence of end-functional polystyrene bearing

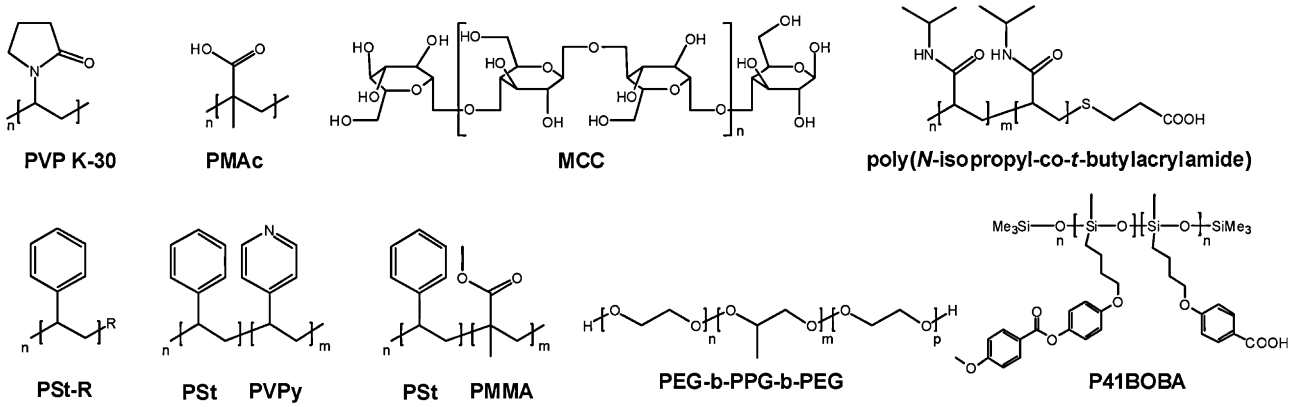

Fig. 5. Polymers used as stabilising agents in the synthesis of Co-NPs.

Table 4
Co-NPs stabilised by polymers.

Entry	Stabilising Agent	Synthetic procedure	Solvent	Co-NPs size	Ref.
1	PVP K-30	$NaBH_4$ reduction of $CoCl_2{\cdot}6H_2O$ at 80 °C	MeOH	7.2 nm	[62]
2	PVP K-30	$NaBH_4$ reduction of $CoCl_2{\cdot}6H_2O$ at r.t.	H_2O	Not specified	[63]
3	PVP-C8	Thermal decomposition of $[Co_2(CO)_8]$	Toluene-squalene	15–30 nm	[64]
4	PVP K-30	$NaBH_4$ reduction of Co salts at r.t.	H_2O	2.9–4.7 nm	[28]
5	PVP K-30	Thermal decomposition of $[Co_2(CO)_8]$	Pentane-H_2O	1.6–1.9 nm	[28]
6	PMAcDDT	$NaBH_4$ reduction of $CoCl_2{\cdot}6H_2O$ r.t.	H_2O	2.0–7.5 nm	[65]
7	MF-4SK	$NaBH_4$ reduction of $CoCl_2{\cdot}6H_2O$ at r.t.	H_2O	3.5 nm	[66]
8	Microcrystalline cellulose (MCC)	NaH_2PO_2 reduction of Co salt at 80 °C	H_2O	5.3–6.3 nm	[67]
9	Poly(N-isopropyl-co-*t*-butylacrylamide)	Thermal decomposition of $[Co_2(CO)_8]$	1,2-Dichlorobenzene	7.0 nm	[68]
10	End-functional polystyrene (PSt-R)	Thermal decomposition of $[Co_2(CO)_8]$	1,2-Dichlorobenzene	18–43 nm	[69]
11	Polystyrene(PSt)-poly-4-vinyl-pyridine (PVPy)	$Li(C_2H_5)_3BH$ reduction of $CoC1_2$ at r.t.	THF	1–5 nm	[70]
12	Polystyrene (PSt)-poly-4-vinyl-pyridine (PVPy)	Thermal decomposition of $[Co_2(CO)_8]$	Toluene	1–5 nm	[70]
13	Poly-(ethylene glycol)-block-poly(propylene glycol)-block-poly-(ethylene glycol) (PEG-b-PPG-b-PEG)	Ethylene glycol (EG) reduction of $CoCl_2$ at 200 °C	EG	13 nm	[74]
14	PVP-K30	$[Co(C_8H_{13})(C_8H_{12})]$ under 3 bar H_2 at 60 °C	THF	1.5–2.0 nm	[39]
15	Poly(2,6-dimethyl-1,4-phenyleneoxide) (PPO)	$[Co(C_8H_{13})(C_8H_{12})]$ under 3 bar H_2 at 60 °C	THF	4.0 nm	[39]
16	P41BOBA	$Co[N(SiMe_3)_2]_2$ under 3 bar H_2 at 60 °C	Toluene	3–14 nm	[75]

either amine (PSt-NH_2), carboxylic acids (PSt-COOH) or phosphine oxide (PSt-Dioctylphosphine oxide, DOPO) ligating moieties (Fig. 5) [69]. The resulting PSt-CoNPs displayed a wide range of mean diameters (between 18 and 43 nm) and showed organization of dipolar colloids into extended nanoparticle chains (entry 10, Table 4). The synthesis of Co-NPs stabilised by amphiphilic block copolymer micelles, such as polystyrene-poly-4-vinyl-pyridine (PSt-4-PVPy) (Fig. 5), was also described (entries 11–12, Table 4) [70]. These Co-NPs were synthesised: (i) by reduction of $CoCl_2$ using $Li(C_2H_5)_3BH$ as reducing agent, and (ii) by thermal decomposition of $[Co_2(CO)_8]$. The authors observed that the small Co-NPs (ca. 1–5 nm) were obtained by both methods. Similar procedures were described for the synthesis of Co-NPs by thermal decomposition of $[Co_2(CO)_8]$ in presence of polystyrene-poly-2-vinyl-pyridine (PSt-2-PVPy) [71], polystyrene-*b*-poly(methylmethacrylate) (PSt-b-PMMA) (Fig. 5) [72], poly[dimethylsiloxane-b-(3-cyanopropyl)-methylsiloxane-b-dimethylsiloxane] (PDMS-PCPMSPDMS) [73]. The formation Co-NPs of 13 nm stabilised by block copolymer poly-(ethylene glycol)-block-poly(propylene glycol)-block-poly-(ethylene glycol) (PEG-b-PPG-b-PEG) (Fig. 5), a biocompatible amphiphilic polymer, was carried out by solvothermal treatment of ethylene glycol solution of $CoCl_2$ (entry 13, Table 4) [74]. These Co-NPs could be dispersed in polar and nonpolar solvents.

Chaudret an co-workers reported the synthesis of Co-NPs by decomposition of $[Co(C_8H_{13})(C_8H_{12})]$ under 3 bar H_2 at 60 °C. They obtained Co-NPs of 1.5–2.0 nm and 4.0 nm using as stabilisers PVP K-30 and poly(2,6-dimethyl-1,4-phenyleneoxide) (PPO) (Fig. 5), respectively (entries 14–15, Table 4) [39]. The same group reported the synthesis of Co-NPs stabilised by liquid crystalline copolymer P41BOBA (Fig. 5) by decomposition of $Co[N(SiMe_3)_2]_2$ in presence of the liquid crystalline copolymer under 3 bar of H_2 at 150 °C (entries 16, Table 4) [75]. The authors observed that the BOBA:Co ratio highly affected the shape and size of the obtained Co-NPs. For equimolar BOBA:Co ratios, monodisperse spherical Co-NPs of 10 ± 2 nm were obtained. When the BOBA: Co ratio was decreased to 0.65, small spherical Co-NPs of 3 ± 1 nm were formed together with larger particles of 12 ± 3 nm mean size, while long reaction times produced only well monodisperse spherical 14 ± 2 nm Co-NPs.

4.2. Ionic surfactants

Water-soluble Co-NPs of 4 nm were synthesised by $NaBH_4$ reduction of $CoCl_2{\cdot}6H_2O$ at room temperature in presence of di-dodecyl-di-methylammonium bromide (DDAB) (Fig. 6) [76]. Co-NPs of 7.5–9.0 nm were formed by $NaBH_4$ reduction at room temperature of $CoCl_2{\cdot}6H_2O$ in presence of dodecyl-*N*,*N*-di-methyl-3-ammonio-1-propanesulfonate (SB12) (Fig. 6) [77]. 6.4 nm Co-NPs with a polydispersity of 21% were formed by $NaBH_4$ reduction at room temperature of $[Co(OAT)_2]$ (OAT = (2-ethylhexyl)sulfosuccinate) [78]. Sodium (2-ehtylhexyl)sulfosuccinate was formed during the reaction and acts as a stabilising agent (Fig. 6).

4.3. Ionic liquids

Co-NPs were synthesised by thermal decomposition of $[Co_2(CO)_8]$ dissolved in different imidazolium cations (1-*n*-butyl-3-methylimidazolium [BMI], 1-*n*-decyl-3-methylimidazolium [DMI]) and anions (PF_6-NTf_2-BF_4-FAP) as stabilising agents (Fig. 7) [48b,79–82]. The authors observed that using 1-*n*-decyl-3-methylimidazolium *N*-bis(trifluoromethanesulfonyl)-imidate [DMI·NTf_2] as stabilising agent, Co-NPs with a binomial size distribution were formed (79 ± 17 nm and 11 ± 3 nm, respectively) (entry 1, Table 5). Using 1-*n*-decyl-3-methylimidazolium trifluoro-tris-(pentafluoroethane) phosphate [DMI·FAP], Co-NPs of 53 ± 22 nm were obtained after 5 min and longer reaction times (ca. 300 min) produced Co-NPs of 5.5 ± 1.1 nm (entry 2, Table 5).

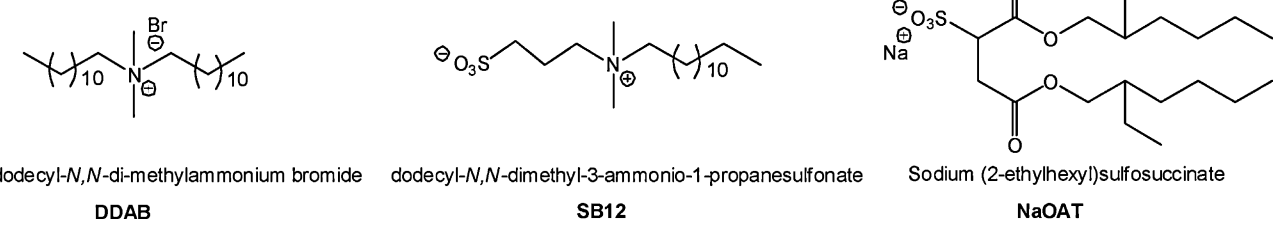

N,*N*-di-dodecyl-*N*,*N*-di-methylammonium bromide — **DDAB**

dodecyl-*N*,*N*-dimethyl-3-ammonio-1-propanesulfonate — **SB12**

Sodium (2-ethylhexyl)sulfosuccinate — **NaOAT**

Fig. 6. Surfactants used as stabilising agents in the synthesis of Co-NPs.

Table 5
Co-NPs synthesised by decomposition of $[Co_2(CO)_8]$ in presence of imidazolium ionic liquids.

Entry	Stabilising agent	Synthetic procedure	Co-NPs size	Ref.
1	1-*n*-Decyl-3-methylimidazolium N-bis(trifluoro methanesulfonyl)imidate [DMI·NTf_2]	Thermal decomposition at 150 °C	Binomial distr.: 11 nm and 79 nm	[81]
2	1-*n*-Decyl-3-methylimidazolium trifluoro-tris-(pentafluoroethane)phosphate [DMI·FAB]	Thermal decomposition at 150 °C	53 nm (5 min) 5.5 nm (300 min)	[81]
3	1-*n*-Decyl-3-methylimidazolium tetrafluoroborate [DMI·BF_4]	Thermal decomposition at 150 °C	4.5 nm	[80]
4	1-*n*-Butyl-3-methylimidazolium N-bis(trifluoro methanesulfonyl)imidate [BMI·NTf_2]	Thermal decomposition at 150 °C	7.7 nm	[80]
5	1-*n*-Butyl-3-methylimidazolium tetrafluoroborate [BMI·BF_4]	Thermal decomposition at 100 °C	14 nm	[54]
6	1-*n*-Butyl-3-methylimidazolium tetrafluoroborate [BMI·BF_4]	Microwave irradiation	5.1 nm	[54]
7	1-*n*-Butyl-3-methylimidazolium tetrafluoroborate [BMI·BF_4]	Photocatalytic decomposition	8.1 nm	[54]

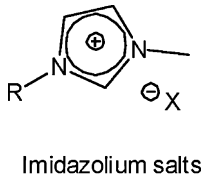

Fig. 7. Ionic liquids used as stabilising agents in the synthesis of Co-NPs.

Interestingly, smaller Co-NPs with irregular shape were obtained using as stabilising agents 1-*n*-decyl-3-methylimidazolium [DMI·BF_4] and 1-*n*-butyl-3-methylimidazolium [BMI] ILs associated with NTf_2^-, FAP^-, and BF_4^- ions (entries 3–4, Table 5).

Co-NPs of 5.1, 8.1 and 14 nm were synthesised by decomposition of the $[Co_2(CO)_8]$ in presence of [BMI·BF_4] using microwave irradiation, photocatalytic treatment and thermal treatment at 100 °C (entries 5–7, Table 5) [54].

4.4. Small molecules

Small molecules containing donor sites, currently used as ligands in coordination chemistry, were probed to be efficient stabilising agent for the synthesis of Co-NPs [83–91]. These type of Co-NPs could be synthesised by reduction of metallic salts or decomposition of organometallic precursors, such as $[Co_2(CO)_8]$, $[Co(C_8H_{13})(C_8H_{12})]$ and $Co[N(SiMe_3)_2]_2$. For instance, Co-NPs of mean diameter 6.5–9.5 nm stabilised by oleic acid and triphenylphosphine were synthesised by $LiBEt_3H$ reduction of $CoCl_2$ [85]. The thermal decomposition of $[Co_2(CO)_8]$ in presence of a mixture of oleic acid/trioctylphosphine oxide produced Co-NPs of 4.5–9.5 nm [87,89]. The decomposition of $[Co(C_8H_{13})(C_8H_{12})]$ by H_2 reduction (3 bar) at room temperature in presence of a mixture of oleic acid and octylamine, oleic amine and hexadecylamine produced Co-NPs of 1.5, 4.0 and 25 nm, respectively [90]. The decomposition of $Co[N(SiMe_3)_2]_2$ by H_2 reduction (3 bar) at 150 °C using hexadecylamine and lauric acid as stabilising agents produced Co-NPs of about 4 nm and nanorods of 90 nm mean length and 5.5 nm diameter.

5. Stabilisers used for the synthesis of colloidal Fe-nanoparticles

5.1. Polymers

Fe-NPs of 6.0 ± 1.3 nm were synthesised by $NaBH_4$ reduction of $FeCl_3{\cdot}6H_2O$ at pH 9.5 in the presence of polyacrylic acid (PAAc) (Fig. 8) as stabilising agent and palladium ions as seeds (entries 1–2, Table 6) [92]. The authors observed that at lower pH (ca. 8.75), Fe-NPs of 59 nm were obtained. However, in the absence of palladium ions, the mean diameter of Fe-NPs is 110 nm.

Fe-NPs of 1.6 nm were formed by $NaBH_4$ reduction of $FeCl_3{\cdot}6H_2O$ in the presence of poly(acrylic acid) (PAAc)/poly(vinyl alcohol) (PVA) (Fig. 8) nanofibers as stabilising agent (entry 3, Table 6) [93]. The same authors reported the synthesis of 1.6 nm

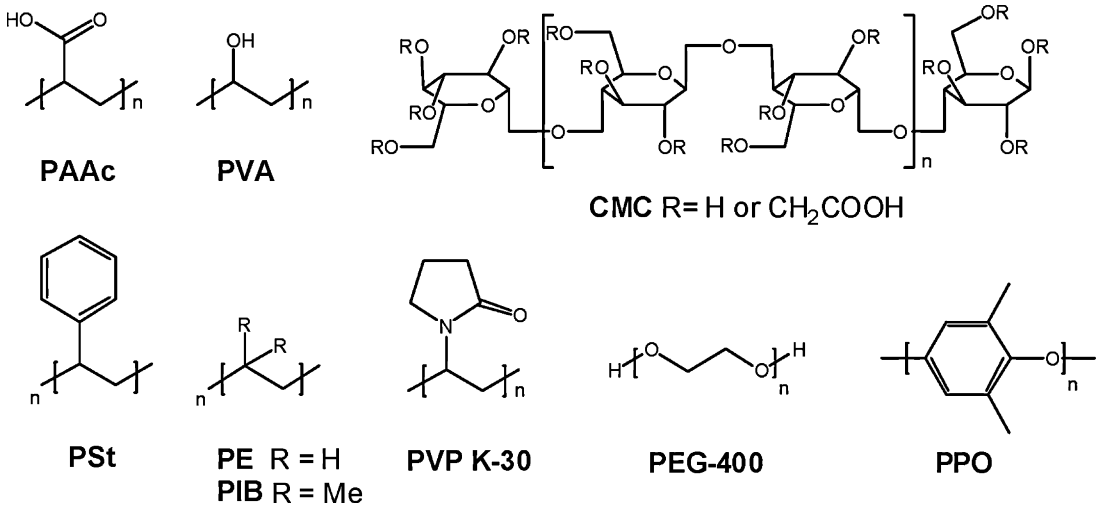

Fig. 8. Polymers used as stabilising agents in the synthesis of Fe-NPs.

Table 6
Fe-NPs stabilised by polymers.

Entry	Stabilising agent	Synthetic procedure	Solvent	Fe-NPs size	Ref.
1	Polyacrylic acid (PAAc)	$NaBH_4$ reduction of $FeCl_3{\cdot}6H_2O$ at r.t.	H_2O	110 nm	[92]
2	Polyacrylic acid (PAAc)	$NaBH_4$ reduction of $FeCl_3{\cdot}6H_2O$ and Pd ions as seeds at r.t.	H_2O	6.0 nm (pH = 9.5) 59 nm (pH = 8.75)	[92]
3	Poly(acrylic acid) (PAAc)/poly(vinyl alcohol) (PVA)	$NaBH_4$ reduction of $FeCl_3{\cdot}6H_2O$ at r.t.	H_2O	1.6 nm	[93,94]
4	Poly(vinyl alcohol-co-vinyl acetate-co-itaconic acid) (PV3A)	$NaBH_4$ reduction of $FeCl_3{\cdot}6H_2O$ at r.t.	H_2O	15.5 nm	[95]
5	Carboxymethyl cellulose (CMC)	$NaBH_4$ reduction of $FeSO_4{\cdot}7H_2O$ at r.t.	H_2O	18.1–94 nm	[96,97]
6	PolyFlo	$NaBH_4$ reduction of $FeSO_4{\cdot}7H_2O$ at r.t.	H_2O	10–30 nm	[98]
7	PVP K-30	Sonolysis of $[Fe(CO)_5]$	Octanol	3–8 nm	[99]
6	Poly(ethylene glycol)-400 (PEG-400)	Sonolysis of $[Fe(CO)_5]$	Hexadecane	3 nm	[100]
8	Polyisobutylene (PIB) functionalized with tetraethylenepentamine (TEBA)	Thermal decomposition of $[Fe(CO)_5]$	Kerosene	8–20 nm	[101]
9	Polyethylene (PE) functionalized with tetraethylenepentamine (TEBA)	Thermal decomposition of $[Fe(CO)_5]$	Kerosene	16 nm	[101]
10	Polystyrene (PSt) functionalized with tetraethylenepentamine (TEBA)	Thermal decomposition of $[Fe(CO)_5]$	Kerosene	24–50 nm	[101]
11	Poly(2,6-dimethyl-1,4-phenyleneoxide) (PPO)	Decomposition of $Fe[N(SiMe_3)_2]_2$ under 3 bar H_2 at 110 °C	Toluene	1.8 nm	[102]

Fe-NPs by $NaBH_4$ reduction of $FeCl_3{\cdot}6H_2O$ in presence MWCNT-incorporated PAAc/PVA nanofibers [94].

Fe-NPs of ca. 15.5 nm were synthesised by $NaBH_4$ reduction of $FeCl_3{\cdot}6H_2O$ in presence of poly(vinyl alcohol-co-vinyl acetate-co-itaconic acid) (PV3A), a non-toxic biodegradable polymer (entry 4, Table 6) [95]. Fe-NPs of 18.1 ± 2.5 nm and 94 ± 25 nm were synthesised by $NaBH_4$ reduction of $FeSO_4{\cdot}7H_2O$ in presence of carboxymethyl cellulose (CMC) (Fig. 8) (entry 5, Table 6) [96,97]. Fe-NPs of 10–30 nm were synthesised by $NaBH_4$ reduction of $FeSO_4{\cdot}7H_2O$ in presence of PolyFlo, a hydrophobic polymer resin (entry 6, Table 6) [98].

Fe-NPs of 3–8 nm were synthesis by sonolysis of $[Fe(CO)_5]$ in presence of PVP K-30 (Fig. 8) as stabilising agent (entry 7, Table 6) [99]. Fe-NPs of 3 nm stabilised by poly(ethylene glycol)-400 (PEG-400) (Fig. 8) were formed by sonolysis of $[Fe(CO)_5]$ (entry 7, Table 6) [100]. Fe-NPs stabilised by polyisobutylene (PIB) (Fig. 8), polyethylene (PE) (Fig. 8), or polystyrene (PSt) (Fig. 8) chains functionalized with tetraethylenepentamine (TEBA) were synthesised by thermal decomposition of $[Fe(CO)_5]$ (entries 8–10, Table 6) [101]. PIB-TEBA stabilised Fe-NPs of various sizes (ca. 8, 12, 18 and 20 nm) as a function of the ratio polymer/metal. Similar sizes (ca. 16 nm) were obtained using PE-TEBA as stabilising agent whereas PSt-TEBA produced larger Fe-NPs (ca. 24–50 nm). Fe-NPs of 1.8 nm were synthesised by decomposition of $Fe[N(SiMe_3)_2]_2$ under 3 bar H_2 at 110 °C in presence of by poly(2,6-dimethyl-1,4-phenyleneoxide) (PPO) (Fig. 8) (entry 11, Table 6) [102].

5.2. Ionic surfactants

Fe-NPs of 4.2 nm were synthesised by $LiBH_4$ reduction of $Fe(BF_4)_2$ in presence of *N*-dodecyl-*N*,*N*,*N*-tri-methylammonium bromide (DTAB) (Fig. 9) [103].

5.3. Ionic liquids

Fe-NPs of 8.6, 7.0 and 5.2 nm were synthesised by decomposition of $[Fe_2(CO)_9]$ in presence of 1-*n*-butyl-3-methylimidazolium tetrafluoroborate [BMI·BF_4] (Fig. 10) using microwave irradiation, photocatalytic treatment and thermal treatment at 100 °C (entries 1–3, Table 7) [54,104]. Fe-NPs of 3.00 ± 0.80 nm stabilised by 1-*n*-butyl-3-methylimidazolium tetrafluoroborate [BMI·BF_4], 1-*n*-butyl-3-methylimidazolium hexafluorophosphate [BMI·PF_6] and 1-*n*-butyl-3-methylimidazolium N-bis(trifluoro methanesulfonyl)imidate [BMI·NTf_2] were synthesised by sonolysis of $[Fe(CO)_5]$ (entries 4–6, Table 7) [105]. Fe-NPs of mean diameters between 1 and 3 nm stabilised by 1-butyl-1-methylpyrrolidinium N-bis(trifluoro methanesulfonyl)imidate [BMP·NTf_2] (Fig. 10) were synthesised by potentiostatic cathodic reduction of $Fe[NTf_2]_2$ (entries 7, Table 7) [106].

5.4. Small molecules

Small molecules containing coordinating atoms were probed to be efficient stabilising agent for the synthesis of Fe-NPs. These type of Fe-NPs are synthesised by reduction of metallic salts or decomposition of organometallic precursors, such as $[Fe(CO)_5]$, [Fe(OAT)] (TOA = 2-ethyl-hexylsulfosuccinate), $Fe(acac)_3$ and $Fe[N(SiMe_3)_2)_2]$.

For instance, Fe-NPs of 8 nm were synthesised by $NaBH_4$ reduction of $FeCl_2{\cdot}4H_2O$ using EG as a solvent [63]. Fe-NPs were also synthesised by KBH_4 reduction of $FeCl_3{\cdot}6H_2O$ using H_2O, EG and H_2O/EG mixtures as the reaction medium [107]. Smaller Fe-NPs (ca. 3–8 nm) were formed using EG as a solvent than in H_2O/EG mixtures and H_2O (20–45 and 30–60 nm, respectively). Fe-NPs of 5–15 nm were obtained by reduction of Fe salts, such as $Fe(NO_3)_3$, $FeCl_3$ and $FeSO_4$, in presence of caffeine/polyphenols [108]. The formation of Fe-NPs with caffeine/polyphenols occurs via the following steps: (i) complexation with Fe salts, (ii) simultaneous reduction of Fe(III) capping with oxidized polyphenols/caffeine.

Fe-NPs of 4–9 nm and 7–11 nm were synthesised by reacting 4-MeC_6H_4MgBr with $FeCl_3$-phosphine ligands and $FeCl_3$-PEG, respectively [109]. These Fe-NPs were successfully applied as nanocatalysts for the cross-coupling of aryl Grignard reagents. Fe-NPs of 2.67 ± 0.60 nm were prepared by reducing $FeCl_3$ with organomagensium reagents in THF. These Fe-NPs were successfully

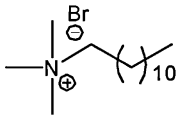

N-dodecyl-*N*,*N*,*N*-tri-methylammonium bromide

DTAB

Fig. 9. Surfactants used as stabilising agents in the synthesis of Fe-NPs.

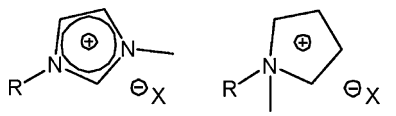

Imidazolium salts Pyrrolidinium salts

Fig. 10. Ionic liquids used as stabilising agents in the synthesis of Fe-NPs.

Table 7
Fe-NPs stabilised by ionic liquids.

Entry	Stabilising agent	Synthetic procedure	Fe-NPs size	Ref.
1	1-*n*-Butyl-3-methylimidazolium tetrafluoroborate [BMI·BF_4]	Thermal decomposition of [$Fe_2(CO)_9$] at 100 °C	5.2 nm	[54,104]
2	1-*n*-Butyl-3-methylimidazolium tetrafluoroborate [BMI·BF_4]	Microwave irradiation of [$Fe_2(CO)_9$]	8.6 nm	[54]
3	1-*n*-Butyl-3-methylimidazolium tetrafluoroborate [BMI·BF_4]	Photocatalytic decomposition of [$Fe_2(CO)_9$]	7.0 nm	[54]
4	1-*n*-Butyl-3-methylimidazolium tetrafluoroborate [BMI·BF_4]	Sonolysis of [$Fe(CO)_5$]	3.0 nm	[105]
5	1-*n*-Butyl-3-methylimidazolium hexafluorophosphate [BMI·PF_6]	Sonolysis of [$Fe(CO)_5$]	3.0 nm	[105]
6	1-*n*-Butyl-3-methylimidazolium N-bis(trifluoro methanesulfonyl)imidate [BMI·NTf_2]	Sonolysis of [$Fe(CO)_5$]	3.0 nm	[105]
7	1-Butyl-1-methylpyrrolidinium N-bis(trifluoro methanesulfonyl)imidate [BMP·NTf_2]	Potentiostatic cathodic reduction of Fe[NTf_2]$_2$	1–3 nm	[106]

applied in the hydrogenation of alkenes and alkynes under mild conditions [110,111]. Interestingly, the authors observed that the Fe-NPs synthesised by $NaBH_4$ reduction of Fe salts ($FeCl_3$, $Fe(acac)_3$, $Fe(NO_3)_3$, $FeSO_4$, $FeCl_2$, $FeBr_2$, FeI_2, $Fe(OAc)_2$) produced poor hydrogenation activity.

Fe-NPs of 8 nm and 2 nm were synthesised by sonolysis of [$Fe(CO)_5$] in presence of oleic acid and tryoctylphosphine oxide, respectively [99,112,113]. Fe-NPs of 3 nm were synthesised by $NaBH_4$ reduction of Fe(OAT) ((2-ethylhexyl) sulfosuccinate) in presence of trioctylphosphine oxide [114]. Fe-NPs of 15–20 nm were synthesised by polyol reduction of $Fe(acac)_3$ in presence of oleic acid [115]. Fe-NPs of 5–7 nm were synthesised by decomposition of Fe[$N(SiMe_3)_2$]$_2$ under 3 bar H_2 at 150 °C using long-chain amines and organic acids [102,116].

6. Fischer–Tropsch reaction: supported catalysts vs. soluble nanocatalysts

Only Co- and Fe-based catalysts can be considered as practical for industrial application in FT synthesis [117]. The three South African F-T plants currently use Fe based catalysts while Shell's Malaysian plant uses cobalt based ones [117]. Because Co is so much more active than Fe, future plants aiming at diesel fuel production will probably use Co based catalysts [117]. For the production of the high value linear alkenes, however, Fe catalysts, operating at high temperatures in fluidized bed reactors or at low temperature for the conversion of coal-derived syngas will remain the catalyst of choice. Concerning Ru based catalysts, their higher stability and their superior catalytic performance under mild reaction conditions make it attractive for their study at laboratory scale.

Supported catalysts and soluble nanocatalysts have been widely investigated over the last 80 years or more [118]. The first type presents the advantage of easy recycling of the nanocatalysts while the second is expected to exhibit greater catalytic performances since reducing the particle size of the catalyst to several nanometers while maintaining the three-dimensional freedom of the particles may in principle significantly increase the catalytic activity as well as decrease the working temperature for the process.

Supported catalysts are the most widely employed type in F-T. The most common supports are SiO_2 [119–131] and Al_2O_3 [124,125,130,132–136]. Alternatively, other inorganic oxides such as TiO_2 [119,124,137,138], charcoal supports such as carbon nanotubes (CNT) [119,134c,139,140], carbon nanofibers (CNF) [141], activated carbon (AC) [119,142], and mesoporous materials such as SBA [127], ZSM [143], HZSM [138b] and ITQ [144], have been used.

In contrast with the traditionally supported M-NPs, the soluble nanocatalysts are freely rotational and three-dimensional in reaction systems. Thus, their metal-surface active sites are much more accessible for the reactant molecules, which enhance their activity [145]. Their synthesis and their successful application in FT-processes was recently reported [27,28,63,64,80,81,107]. These studies revealed that the catalytic performance of these systems is highly affected by the nature of the stabilising agent and the solvent as well as by the size and shape of the M-NPs. In this section, after examining the results obtained using supported FT-catalysts, the solvent and NPs size and shape effect will be described.

6.1. Supported catalysts

In Tables 8 and 9, the activity and selectivity obtained with the traditional F-T catalysts are listed. Due of the large differences in catalyst preparation methods and F-T reaction conditions reported, it is very difficult to compare the catalytic results described in the literature for each type of catalyst. In the next section, after examining the most general results obtained using each type of metal catalysts, the most important trends reported in the literature are described and ordered by metal and compared considering the nature of the catalyst support.

The Ru/SiO_2 catalysts produced activities up to 1.22 mol_{CO} mol_{Ru}^{-1} h^{-1} (entry 1 and 2, Table 8) [121,122]. In the case of Co, the activities varied between 7.40 and 0.30 mol_{CO} mol_{Co}^{-1} h^{-1} as a function of the nature of the support and the reaction temperature (entries 3–7, Table 8) [123d,126,132,134g,136b]. The highest activities were reported using CNF and Al_2O_3 as supports. For Fe catalysts, activities between 2.00 and 0.30 mol_{CO} mol_{Fe}^{-1} h^{-1} were reported (entries 8–10, Table 8) [129e,139,146]. In terms of C_5^+ selectivity, the Ru and Co supported catalysts are usually much more selective towards C_5^+ products than their Fe counterparts (entries 1–9 vs. entries 10–12, Table 9). In the case of Ru, C_5^+ selectivities up to 83 wt% were obtained using SiO_2 and AC supported catalysts (entries 1 and 4, Table 9) [119]. In contrast, with TiO_2 and CNT supported catalysts, lower C_5^+ selectivities were achieved (ca. 60 wt%) (entries 2 and 3, Table 9) [119]. For Co, C_5^+ selectivities up to 90 wt% were reported using supported catalysts onto SiO_2, Al_2O_3, CNF and CNT (entries 5, 6, 8 and 9, Table 9) [126,134c,140b]. It should be noted that much lower C_5^+ selectivities (30 wt%) (entry 7, Table 9) were obtained when the Co/TiO_2 catalysts were used [137b]. In the case of Fe nanocatalysts, higher C_5^+ selectivities were achieved with Al_2O_3 supported catalysts than with their CNF and CNT counterparts (entries 10–12, Table 9) [136,139,142].

6.1.1. Ru supported catalysts

Claeys et al. observed that the addition of water over a Ru/SiO_2 catalyst during FT led to a significant increase in product formation rates, significant lower methane selectivity and improvement in chain growth [121]. Upon increasing water partial pressures, the total product distribution shifted from Anderson–Schulz–Flory (ASF) distributions to a much narrower distribution. An additional product formation route by combination of adjacent alkyl chains to form paraffins has been proposed. These findings were discussed in connection with the crucial mechanistic role of water as a moderator in the kinetic regime of the FT.

Dumesic et al. reported the catalytic conversion of glycerol to syngas coupled with F-T in a two-bed reactor system that contain a Pt–Re/C catalyst bed followed by a Ru/TiO_2 catalyst bed. This

Table 8
Activities reported for metal supported FT catalysts.

Entry	Catalyst	T/°C	Activity/mol_{CO} mol_{M}^{-1} h^{-1}	Ref.
1	Ru/SiO_2	200	1.22	[121]
2	Ru/SiO_2	150	0.19	[122]
3	Co/SiO_2	200	2.75	[123d]
4	Co/SiO_2	190	0.33	[126]
5	Co/Al_2O_3	190	3.30	[132]
6	Co/Al_2O_3	180	0.80	[134g]
7	Co/CNF	220	7.40	[141b]
8	$Fe–Cu–K/SiO_2$	250	2.00	[129e]
9	Fe/CNT	220	0.73	[140]
10	$Fe_2O_3–K_2O/CuO$	250	0.30	[146]

combined process produced liquid alkanes with more than 40 wt% of the carbon in the C_5^+ products [137]. Recently, Wang et al. described a comparison between the catalytic performance of various Ru supported catalysts, such as Ru/SiO_2, Ru/TiO_2, Ru/ZrO_2, Ru/MgO, Ru/NaY, Ru/HY, Ru/H-beta, Ru/AC, Ru/graphite and Ru/CNT under identical catalytic conditions [119]. They found that Ru/CNT is a highly selective FT catalyst for the formation of $C_{10}–C_{20}$ hydrocarbons. The unique hydrogen adsorption properties and the acidic functional groups on the CNT surfaces may both play a role to form $C_{10}–C_{20}$ products by mild hydrocracking of heavier hydrocarbons. Both the $C_{10}–C_{20}$ selectivity and the TOF for CO conversion were found to depend on the mean size of the Ru-NPs, with a size of approximately 7 nm exhibiting the best C_{10} selectivity and higher TOF.

6.1.2. Co supported catalysts

Miseo et al. demonstrated that the control of support/surface interactions is a key parameter for obtaining optimum dispersions, reducibility, and metal distribution in FT catalysts [123e]. They described several examples of improvements in Co/SiO_2 and Co/TiO_2 dispersion by varying synthetic parameters and stabilising methods. Tennant et al. reported the use of Co/SiO_2 to develop a slurry-phase reactor which is incorporated into an integrated gasification and combined cycle complex in order to coproduce electricity, fuels, and chemicals [123d]. Shull et al. described the preparation of a series of $Co–Ru–Zr/SiO_2$ catalysts in order to gain understanding on the effects of calcination temperatures on their stability and activity in FT [123a]. When the catalysts were calcinated at lower temperature (ca. 300 °C) in the presence of chlorine, lower crystallite size and thus better catalytic activity in FT were achieved. Le Courtous et al. used a channel microreactor with a wall-coated Co/SiO_2 catalyst in FT and reported that with this method, only moderate C_5^+ selectivity was achieved [123b]. Asami et al. described the production of *iso*-paraffin-rich hydrocarbons via isomerisation and/or hydrocracking of the primary FT hydrocarbon products using a Co/SiO_2 FT catalysts [126]. A mixture of a small amount of zeolite, Pd/zeolite and Co/SiO_2 enhanced the formation of $C_4–C_{10}$ *iso*-paraffins and reduced the yield in higher molecular hydrocarbons by selectively cracking these hydrocarbons. The effect of mesoporous support structure and cobalt content on Co-NPs dispersion and reducibility was studied by Griboval-Constant using Co/SBA-15 and Co/SiO_2 FT catalysts [128]. Higher FT reaction rates with no changes in the hydrocarbon selectivity were observed using Co/SBA-15. Sun et al. studied the stability of a $Co/ZrO_2/SiO_2$ catalyst in the FT as a function of time on stream [123f]. At long time on stream, the catalyst showed a significant decrease in CO conversion, while the hydrocarbon distribution hardly changed during the experiment. The deactivated catalyst was partially regenerated by flowing H_2 at 400 °C. Using XRD, FT-IR and TGA, hydrated Co-silica mixed species were identified. Thus, the cause of deactivation was proposed to be partly due to the formation of inactive hydrated silicate between Co metal and silica in presence of high partial pressure of water. Baumgartner reported that at high conversion in F-T, thus under hydrothermal conditions, the formation of a Co-silica mixed oxide was induced, thus causing the deactivation of the catalyst [123c]. Fujimoto et al. investigated the influence of solvent on the selectivity to α-olefins as a function of the carbon number in the solvent using a Co/SiO_2 FT catalyst [127]. Hydrocarbons including *n*-hexane, *n*-octane, *n*-decane, *n*-dodecane, *n*-hexadecane, *iso*-octane and decahydronaphthalene were used as solvents. No clear effect on the catalytic activity or chain growth was observed but did exhibit a remarkable influence on the α-olefin–alkane ratio. When *n*-hexane was used as solvent, lower α-olefin selectivity were obtained for the higher hydrocarbons compared to those obtained for lighter hydrocarbons. The use of *n*-decane resulted in the highest α-olefin selectivity independently of the product. This result is due to quicker desorption and diffusion, and slower re-adsorption for primary α-olefin. However, an effect of the lower solubility of the α-olefins in this solvent can not be discarded. In general, the use of *n*-paraffin as solvent yields a higher selectivity to α-olefin than branched paraffin or cyclic paraffin. The use of supercritial *n*-pentane for F-T using α-tetradecene as co-feed was carried out over Co/SiO_2 catalyst and was reported by Fujimoto et al. [123g]. They showed that α-tetradecene could participate in the chain growing

Table 9
C_5^+ selectivity obtained using metal supported FT catalysts.

Entry	Catalyst	P/bar	H_2/CO	T/°C	% CO conv.	% wt C_5^+	Ref.
1	Ru/SiO_2	20	1.0	260	32	83	[119]
2	Ru/TiO_2	20	1.0	260	20	50	[119]
3	Ru/CNT	20	1.0	260	11	60	[119]
4	Ru/AC	20	1.0	260	34	83	[119]
5	Co/SiO_2	10	2.0	240	38	81	[126]
6	Co/Al_2O_3	25	2.0	220	25	90	[134c]
7	Co/TiO_2	10	1.0	250	41	30	[138b]
8	Co/CNT	25	2.0	220	45	86	[134c]
9	Co/CNF	35	2.0	220	67	85	[141b]
10	Fe/Al_2O_3	15	0.67	260	22	75	[136]
11	Fe/CNT	20	2.0	220	10	46	[139]
12	Fe/AC	23	0.9	260	30	30	[142]

process by reaction with the growing chain on the catalyst surface. Indeed, the presence of this compound increases the rate of formation of hydrocarbons larger than C_{14}.

Seehra et al. studied the correlations between the activity and selectivity in the FT using Co/SiO_2 and Co/Al_2O_3 catalysts [125]. They suggested that the pore radius of the catalyst has an influence on both syngas and CO conversions in the gas-phase FT. However, no correlation was observed in the case of supercritical (SC) hexane FT, indicating that mass transfer limitations typically controlled by interparticle characteristics of the catalyst were in this case reduced. This is attributed to the higher solubility of heavy weight products in the SC hexane medium. As a result, the Co catalysts were found to be very stable during SC hexane F-T for relatively long time-on-stream and both the activity and selectivity were found to remain unchanged during the reaction.

Vanhove et al. described the synthesis of Co/Al_2O_3 catalysts and their application in the F-T [134g]. These catalysts were prepared from four commercial aluminas with various Co loadings. The effects of reaction and reduction temperatures, deactivation, cobalt content and structure of supports on the catalytic properties were especially examined. They reported that an increase in the reaction temperature improves the activity and the selectivity for light products. Furthermore, the Co loading and the porosity of supports modify the catalytic properties of these systems by affecting the reducibility of the metal since an increase in the extent of reduction improves the activity and the selectivity for high molecular hydrocarbons. Roberts et al. reported the use of Co/Al_2O_3 and $Co\text{-}Pt/Al_2O_3$ catalysts in the F-T using supercritical hexane and pentane as solvents [134e,f]. They suggested that both supercritical solvents performed almost identically in terms of hydrocarbon product distribution. However, higher CO conversion was obtained using pentane due to the pressure effects on the kinetics [134e,f]. Within the investigated range of conditions, the chain-growth probability increases as the pressure increases and the temperature decreases. However, the influence of reaction temperature on the chain growth probability was determined to be more pronounced than that of the effect of pressure. Comparing the hydrocarbon distributions in both SC-phase and gas-phase FT, the authors concluded that the enhanced solubilities of heavy hydrocarbon products in the SC medium improve the vacant-site accessibility for the readsorption of olefins and subsequent chain growth, as well as the elimination of the adsorption layer. Using a $Co–Ru/Al_2O_3$ catalyst, Haghtalab et al. investigated the effect of variables such as temperature, pressure, solvent type, reactant feed composition, and space velocity on the F-T [133a]. Comparison of the experimental data between the gas phase and SC medium showed that higher CO conversion and lower CH_4 and CO_2 selectivities were obtained for F-T in the SC medium. The CO_2 selectivity did not vary in a regular manner by changing the solvent and H_2/CO ratio but increased at higher temperature and $W/F(CO + H_2)$. Furthermore, the product carbon distribution had a similar shape for all type of solvents but shifted to lighter molecular mass compounds when the temperature, the H_2/CO ratio, or the space velocity were increased and when the pressure was decreased.

Dalai et al. compared the F-T catalytic performance of Co/Al_2O_3 and Co/CNT [134c]. They observed that the F-T rate and CO conversion obtained by Co/CNT catalysts were much larger than that obtained with Co/Al_2O_3. Furthermore, the CNT caused a slight decrease in the F-T product distribution to lower molecular weight hydrocarbons. De Jong et al. described the influence of the particle size of Co/CNF catalysts in the range of 2.6–27 nm on the performance in Fischer–Tropsch synthesis [141b]. The TOF value was independent of Co particle size for catalysts with sizes larger than 6 nm. For Co particle size smaller than 6 nm, both the selectivity and the activity was affected by the nanoparticle size. At 35 bar, when the Co particle size was reduced from 16 to 2.6 nm, the TOF decreased from 23×10^{-3} to 1.4×10^{-3} s^{-1} and the C_5^+ selectivity decreased from 85 to 51 wt%.

Holmen et al. studied the F-T catalytic performance of Co/Al_2O_3, Fe/Al_2O_3 and $Co\text{-}Fe/Al_2O_3$ [134a]. They observed that alloying Co with small amounts of Fe improved the F-T activity at low conversion levels when compared to that of the catalyst containing only Co. In contrast, alloying Fe with small amounts of Co lowered the F-T activity compared to that of the Fe catalyst alone, although the relative water-gas-shift (WGS) activity was increased. For the bimetallic catalysts, both F-T and WGS activities rapidly declined at high partial pressure of water due to deactivation by oxidation and sintering. However, the results indicate that WGS and F-T proceeded over sites of different nature in the bimetallic catalysts. The bimetallic catalysts showed essentially no variation in hydrocarbon selectivities and olefin/paraffin ratios compared to the monometallic catalysts, which can be partly explained by the use of a sub-stoichiometric H_2/CO ratio as feed. The lowest C_5^+ selectivity and C_3 olefin/paraffin ratio were obtained using the catalysts containing higher amounts of Fe. Interestingly, the addition of water increased the C_5^+ selectivity and C_3 olefin/paraffin ratio and reduced the CH_4 selectivity. Abatzoglou et al. reported the synthesis of Co, Fe, Co-Fe and Fe-Co catalysts supported on CNT [139]. The monometallic Fe catalyst showed the lowest F-T activity and the highest water–gas shift (WGS) rate. In terms of selectivity, they exhibited the lowest selectivity to C_5^+ hydrocarbons but the highest olefin to paraffin ratio of 1.95. The monometallic Co catalyst exhibited high selectivity (85.1 wt%) towards C_5^+ liquid hydrocarbons, and addition of small amounts of Fe did not significantly change the products selectivity. The Co catalyst with 0.5 wt% Fe showed the highest F-T reaction rate and CO conversion while the olefin to paraffin ratio in the F-T products increased with the addition of Fe. The bimetallic Co–Fe/CNT catalysts proved to be attractive in terms of alcohol formation. The introduction of 4 wt% of Fe in the Co catalyst increased the alcohol selectivity from 2.3 to 26.3 wt%. Kuila et al. observed that the addition of Ru to the $Fe–Co/SiO_2$ catalyst increased CO conversion by 16% but lowered selectivity to propane by 10% [120]. Niemantsverdriet studied the use of a $Co–Pt/Al_2O_3$ F-T catalyst [134b]. In this study, they showed that: (i) there is an increase in carbon deposition with increasing time on stream for wax-extracted cobalt catalysts and that the regeneration of these catalysts is increasingly more difficult at longer time on stream, (ii) this hydrogen resistant carbon has similar reactivity than polymeric carbon. This polymeric-type carbon is located on the support and on cobalt, (iii) removal of the polymeric-type carbon results in a dramatic increase in F-T activity. They conclude that that polymeric carbon deposits is one of the mechanisms which may play a role in the long-term deactivation of Co-based F-T catalysts. Gangwal et al. reported the use of TiO_2 as a support for Co and Fe F-T catalysts [138b]. They observed that the activity of the catalysts prepared from Co, Ni, and Fe on TiO_2 is significantly enhanced if a combination of two metals (forming an alloy) is used as opposed to a single metal. In particular, alloying Co with Ni in a 1:1 ratio gave the highest activity without increasing the selectivity to methane and increasing that to C_5^+ product. Furthermore, the high methanation activity of Ni was significantly suppressed by alloying with either Co or Fe. Adding HZSM-5 to the 50/50 Co–Ni catalyst promoted aromatics formation, decreased methane and C_2 content, reduced olefins, and significantly increased isobutane content. No aliphatic products larger than C_8 were formed. They suggested that by combining the effects of alloying the group VIII metals and a zeolite such as HZSM-5, it might be possible to tailor the selectivity of F-T products.

Holmen et al. compared the F-T catalytic performance of Co-powder, Co-cordierite monolith, Co-steel monolith and Co-alumina monolith [134h]. They found that the Co-cordierite monoliths catalysts are active and selective to C_5^+ as comparable Co-powder

catalysts of small particle size when loaded with relatively low amounts of catalyst. Co-steel monoliths were found to have lower activity and C_5^+ selectivity than powders and cordierite monoliths. Co-alumina monoliths were found to give comparable selectivities to that of Co-powder catalysts but somewhat lower activity.

6.1.3. Fe supported catalysts

Davis et al. described the application of two precipitated Fe catalysts (100 Fe/3.6 Si/0.71 K and 100 Fe/4.4 Si/1.0 K, atomic percent relative to Fe) in a slurry phase F-T [131]. The impact of activation gas, temperature, and pressure on the long-term activity and selectivity of the catalysts was explored. Pre-treatment with CO under the conditions employed gave highly active and stable catalysts. Catalyst performance when synthesis gas activation was used was found to be dependent upon the partial pressure of hydrogen in the activating gas, with low hydrogen partial pressures resulting in the highest catalyst activity ($2.0\,mol_{CO}\,mol_{Fe}^{-1}\,h^{-1}$). Bukur et al. investigated the reduction and the catalytic behaviour of SiO_2 and Al_2O_3-supported Fe F-T catalysts promoted with K and Cu [130]. It was found that the Al_2O_3 inhibits reduction of iron, whereas the reduction behaviour of the SiO_2 supported catalyst was similar to that of the two precipitated Fe-catalysts. Supported and precipitated ($Fe/Cu/K/SiO_2$) catalysts were tested in a stirred tank slurry reactor. Initial activity of the SiO_2-supported catalyst, measured by a value of an apparent first-order reaction rate constant, was 20–40% higher than that of the precipitated Fe-catalysts, whereas the activity of the Al_2O_3-supported catalyst was about 50% less than that of the silica-supported catalyst. SiO_2-supported catalyst had higher gaseous selectivity and lower olefin content than the Al_2O_3-supported catalyst and precipitated catalysts. These results were explained in terms of interactions between potassium with supports, resulting in reduction of the potassium promotion effectiveness.

Prinsloo et al. described the effect of the synthetic methods to form the CNT supported Fe catalysts [140]. These catalysts were prepared by incipient wetness, deposition/precipitation using K_2CO_3, and deposition/precipitation using urea. After reduction, the three catalysts had similar metal surface areas. However, the activity of these catalysts in the F-T differed significantly with the catalyst prepared by incipient wetness being the most active one. It is speculated that the differences in the performance of the catalysts might be attributed to the different crystallite size distributions, which would result in a variation in the amount of the different phases present in the catalyst under reaction conditions. The selectivity in the F-T synthesis over the three catalysts seems to be independent of the method of preparation. Beenackers et al. studied the kinetics of the gas–solid F-T over a commercial $Fe–Cu–K–SiO_2$ in a continuous spinning basket reactor [129e]. Yi et al. reported the incorporation of Al_2O_3 into precipitated Fe catalyst [136]. They observed a strong Fe/Al_2O_3 interaction, which has a significant influence on the surface basicity, reduction and carburization behaviours, as well as F-T performances. Due to this strong interaction, the F-T and WGS activities were decreased by the addition of Al_2O_3. Furthermore, the strong Fe/Al_2O_3 interaction suppresses the reoxidation of iron carbides, stabilises the F-T active sites and improves the catalyst stability. The lower surface basicity also resulted in higher selectivity to light hydrocarbons. Datye et al. studied the effect of activation and reaction treatment on the resulting phase transformations in a $Fe_2O_3–CuO–K_2O$ catalyst [146]. Their results suggested that magnetite has negligible catalytic activity for F-T synthesis whereas carbide formation is necessary before the catalyst becomes active. Furthermore, Ragaini et al. compared the use of Fe/Al_2O_3 and $Fe–K–Cu/Al_2O_3$ in the F-T [135]. They observed that CO conversion, CO_2 and heavy hydrocarbon selectivity increase using higher Fe amounts and in presence of promoters such as K. Two different process regimes, depending on the operative temperature, were observed where either F-T or WGS predominates. Goodwinjr reported that the addition of Cr, Mn, and Zr increased the activity of a precipitated $Fe–Cu/SiO_2$ catalyst for both F-T and WGS reaction and also promoted the dispersion of Fe [129a]. The high activity observed for the Cr-, Mn-, and Zr-promoted Fe catalysts appears to be related to a greater number of active sites. The same authors reported that the addition of K at relatively low concentrations promoted the activity of the Fe/SiO_2 and $Fe–Mn/SiO_2$ catalysts in the F-T and WGS reaction. However, the addition of excess K resulted in the decline of the catalyst activity, probably due to an increased amount of carbon deposition via the Boudouard reaction [129b]. The addition of Mn and/or K increased the concentration of active surface intermediates leading to product. As expected, chain growth probability (α) was enhanced by the presence of K. Similar results were reported by Dadyburjor et al. for Fe/AC F-T catalyst [142]. In this case, the K promoter suppressed the formation of methane and methanol, favoured the formation of higher-molecular-weight hydrocarbons (C_5^+) and alcohols ($C_2–C_5$). Interestingly, the addition of K changes the effect of temperature on the selectivity to oxygenates. In the absence of K, oxygenate selectivity decreases with temperature. However, when K is present, the selectivity is almost independent of the temperature.

6.2. Soluble nanocatalysts

As previously mentioned in this review, FT reactions were effectively catalysed by soluble M-NPs. It is noteworthy that the M-NPs catalytic properties are highly dependent of their size and thus the synthesis of M-NPs with a specific size range and the election of an appropriate stabilising agent are of crucial importance [27,28,63,64,80,81,107]. Furthermore, these catalysts are specifically designed to be applied in low temperature FT processes using slurry type reactors and thus, the choice of a suitable solvent which has to remain liquid under reaction conditions is crucial [117].

In this section, the application of soluble M-NPs as FT catalysts is reviewed with special interest on the M-NPs size, the reaction solvent and the stabilising agent.

6.2.1. Size

Decreasing particle size to the nanometer increases the surface area on which the reaction is carried out. The concentration of low coordinated sites (defect sites) is relatively abundant in nanomaterials providing higher activities due to the lower activation barrier for reactant molecules, which are otherwise negligible or absent in bulk systems [147]. However, it is clear that size dependence in catalysis is much more complex than what this initial hypothesis suggests and there is no single theory that can explain all the phenomena observed. It is believed that the surface atoms or a combination of surface atoms should possess certain ‘geometries’ with required ‘electronic’ properties which enables the surface to act as an efficient catalyst [148,149]. Electronic effects indicate the nature and strength of the bond between the d-band orbital of the surface atom, and the molecular orbitals of the reactants and the products. The surface atoms in different environments have different local electronic structures and interact differently with adsorbate molecules. In general, the d-band centre, which is the first moment of the density of states, projected against the d-orbitals for the surface atoms interacting with the adsorbates as a reactivity descriptor. Transition metal surface with open surface and low coordination number atoms (like steps, edges, kinks and corners) have higher lying d-states and tend to interact strongly with adsorbates. Geometric effects result in a minimum ensemble of atoms with a specific arrangement for adsorption and for the reaction to take place. M-NPs of various morphologies and sizes possess different edge and vertex atoms, and fractions of different crystallographic orientations.

For Ru catalysts, Kou and co-workers reported the synthesis of colloidal Ru-NPs of various sizes (ca. 1.8, 2.0, 2.5, 2.9, 3.3 and 4.0 nm) using the seeded growth method and their application as nanocatalysts in the Fischer–Tropsch synthesis [27]. They observed that the Ru-NPs of 2.0 nm produced higher activities than those obtained using smaller and larger Ru-NPs. Similarly, we observed that the Ru-PVP-NPs of 1.9 nm are more active than the Ru-PVP-NPs of 2.2 and 2.5 nm [28].

Concerning Co catalysts, this size effect has been studied only for Co-supported Fischer–Tropsch catalysts [15c,141b,144,150,151,152]. For the conventionally prepared supported catalysts, the size of the Co particle catalysts is: (a) 20–40 nm for Co/SiO_2 [152g,h,153], and (b) 5–10 nm for Co/Al_2O_3 [154]. Turnover frequencies (TOF) of these catalysts were similar and almost independent of size of Co-NPs when they were larger than 10 nm [150]. The size effect was observed in a small particle range (2–10 nm) for Co supported on carbon nanofiber [141b] and ITQ-2 [144]. The optimal Co-NPs size is relatively large (ca. 7 nm) with smaller Co-NPs exhibiting lower rates even though the exposed metal surface should be much larger [141b,144,155]. The lower activity of the smaller Co-NPs was attributed to: (a) the formation of spinels between the Co and the support oxides, which lock up the Co in a non-reducible form [156], and (b) the fact that smaller Co particles tend to be oxidized [124,155c,157]. Today, the study of the Co-NPs size effect is an active area of research due to the controversy about the easier oxidation of the smaller NPs since bulk thermodynamics would indicate that Co should remain metallic under Fischer–Tropsch reaction conditions [158].

Concerning Fe catalysts, the effect of the mean diameter over the Fischer–Tropsch performance was much less studied. However, it is well-accepted that nanosized Fe particles were essential to achieve high Fischer–Tropsch activity and the mean diameter of these Fe-NPs highly affected the product distributions [159].

6.2.2. Solvent

Recently, the solvent effect in the Fischer–Tropsch process catalysed by colloidal M-NPs was studied using as a solvents: (a) liquid water, (b) ionic liquids and (c) high boiling point organic solvents.

Water is cheap, readily available, nontoxic, non-flammable and environmentally friendly [160]. Furthermore, H_2O is a suitable solvent for many reactions due to: (a) inertness against oxidation and reduction, (b) high polarity, and (c) high solvatation ability. In the case of the Fischer–Tropsch process, the hydrocarbon product is immiscible with water, so the fuel can be easily separated from the catalysts facilitating the work-up process.

It is well established that in the case of the Ru catalysts, the presence of water in the reaction media produced higher activities, lower methane production and narrower product distributions [27,121,150,161,162]. For example, the activity (calculated on the basis of the total number of Ru atoms) of the 5 wt% Ru/SiO_2 catalyst was increased by a factor of 3 when the H_2O pressure was increased from 0.017 to 0.454 MPa [161]. To the best of our knowledge, aqueous-phase Fischer–Tropsch using colloidal Ru-NPs has been only reported by Kou and co-workers [27]. They found that water-soluble Ru-NPs stabilised by PVP are more active Fischer–Tropsch catalysts (ca. 6.90 $mol_{CO}\ mol_{Ru}^{-1}\ h^{-1}$) than the conventional supported catalysts. A 35-fold increase in activity was observed for unsupported Ru-NPs at 150 °C with C_5^+ selectivity up to 84 wt%. In the same way, we studied the application of water-soluble Ru-PVP-NPs in the Fischer–Tropsch synthesis obtaining comparable results in terms of activity and C_5^+ selectivity to those obtained by Kou and co-workers. However, we detected the formation of oxygenated compounds together and CO_2 [28].

The effect of the water is not well established for the Co based Fischer–Tropsch catalysts [27b,63,154b,161–176]. In the case of supported Co catalysts, the effects of water on the Fischer–Tropsch performance depend on the nature of the support, Co metal loading, its promotion with noble metals, and preparation procedure [150,162]. The water effects are reported to be either negligible, negative, or positive. The positive effects of water on the catalyst activity are to facilitate intra-particle transport of syngas and hydrocarbons improving the reaction kinetics. The effect of water on the selectivity of the reaction is probably due to the fact that: (a) hydrocracking processes operate under these conditions, and/or (b) the solubility of the olefins in water decreases when the number of carbon increases, and therefore water could affect the termination step by displacing the less soluble products from the aqueous phase [124,163b]. It is observed, that the presence of water produced an increase in CO conversion, a decrease in methane selectivity and the inhibition of the secondary hydrogenation of olefin products caused by the competitive adsorption of water. The water negative effect is related to the formation of inactive Co oxides or the formation of irreducible cobalt species [124]. In the case of Fe, a negative effect was described since the presence of water produced the deactivation of the catalyst by oxidation and/or sintering [27b,124,150,162].

Recently, Kou and co-workers reported the synthesis of water soluble Co-NPs by KBH_4 reduction of $Co(AcO)_2{\cdot}6H_2O$ using PVP as stabilising agent obtaining activities up to 0.12 $mol_{CO}\ mol_{Co}^{-1}\ h^{-1}$ [63]. They had previously patented: (a) Co catalysts formed by H_2 treatment of $CoCl_2{\cdot}6H_2O$ at 170 °C in presence of PVP produced activities up to 0.020 $mol_{CO}\ mol_{Co}^{-1}\ h^{-1}$, and (b) Fe catalysts formed by H_2 treatment of $FeCl_3{\cdot}6H_2O$ at 200 °C in presence of PVP produced activities up to 0.0096 $mol_{CO}\ mol_{Fe}^{-1}\ h^{-1}$ [27b]. Recently, Wu and co-workers reported the synthesis of Fe-NPs by KBH_4 reduction of $FeCl_3{\cdot}6H_2O$ at room temperature [107]. Fe-NPs of 3–8 nm, 20–40 nm and 30–60 nm were formed using ethyleneglycol (EG), water/EG mixtures and water as a solvent, respectively. These Fe-NPs were applied as catalysts in the Fischer–Tropsch synthesis achieving higher activities using water as a solvent (0.83 $mol_{CO}\ mol_{Fe}^{-1}\ h^{-1}$) than those obtained using water/EG mixtures and EG as a solvent (0.76 and 0.30 $mol_{CO}\ mol_{Fe}^{-1}\ h^{-1}$, respectively). Based on Mössbauer spectra results, the authors correlated the high activity of the water soluble Fe-NPs whit the high content of iron carbides of this catalyst. Concerning the Fischer–Tropsch selectivity, they reported CO_2 selectivity up to 30 mol%, CH_4 selectivity up to 13 wt%, light hydrocarbon (C_2–C_{10}) selectivity up to 70 wt% and C_{21}^+ selectivity up to 0.96 wt%.

Ionic liquids were revealed as a suitable solvent for their use in catalysis due to: (a) their physico-chemical properties, (b) their negligible vapor pressure, (c) relative low viscosity, (d) high thermal, chemical and electrochemical stabilities, and (e) their tunable miscibility of ILs [27,47–57,79–82,104–106,160]. Furthermore, some reactions catalysed by M-NPs exhibit unusual but desired selectivity patterns when performed in ILs [160]. To date, only few examples described the use of ionic liquids as stabilisers for the synthesis of effective Fischer–Tropsch catalysts. Kou and co-workers reported the application in Fischer–Tropsch of the Ru-NPs stabilised by PVP modified with imidazolium salts using 1-*n*-butyl-3-methylimidazolium tetrafluoroborate [BMI·BF_4] as a solvent obtaining activities up to 0.55 $mol_{CO}\ mol_{Ru}^{-1}\ h^{-1}$ [27]. Dupont and co-workers reported that Co-NPs of 7.7 nm stabilised by 1-*n*-butyl-3-methylimidazolium N-bis(trifluoro methanesulfonyl)imidate [BMI·NTf_2] produced activities up to 0.5 h^{-1} affording mainly hydrocarbons in the liquid phase (7–30 carbons) with a chain growth probability of 0.90 [80]. The same group also reported that Co-NPs of 1-*n*-decyl-3-methylimidazolium N-bis(trifluoro methanesulfonyl)imidate [DMI·NTf_2], which displayed a binomial size distribution with mean diameters 11 nm and 79 nm, produced activities up to 0.2×10^{-5} $mol_{CO}\ g_{Co}^{-1}\ s^{-1}$ (0.42 $mol_{CO}\ mol_{Co}^{-1}\ h^{-1}$) [81]. Interestingly, the hydrocarbons formed in the Fischer–Tropsch

with Co-[DMI·NTf_2]-NPs showed a monomial hydrocarbon distribution centered at C_{12}, in contrast the Co-[BMI·NTf_2]-NPs showed a binomial hydrocarbon distribution (centered at C_{12} and C_{21}). They suggested that these differences could be attributed to the Co-NPs size and shape effect [81].

M-NPs solubilised in high boiling point organic solvents were revealed as a efficient catalysts for the Fischer–Tropsch synthesis [160]. The hydrocarbon product are miscible with these type of solvent thus a distillation work-up process is required. Kou and co-workers reported the synthesis of squalene-soluble Co-NPs stabilised by PVP-C8 and their application in Fischer–Tropsch [64]. The Co-C_8-PVP-NPs exhibited comparable Fischer–Tropsch activity ($1.3\,mol_{CO}\,mol_{Co}^{-1}\,h^{-1}$) to those obtained using supported Co catalysts and Co-NPs in ILs. Kou and co-workers also described the application of Fe-NPs as Ficher–Tropsch catalyst using polyethylene glycol (PEG) as a solvent, obtaining activities up to $1.5\,mol_{CO}\,mol_{Fe}^{-1}\,h^{-1}$ with CO_2 selectivity up to mol%, C_5+ selectivity up to 56.1 wt% and methane selectivity up to 5.6 wt% [63a]. Interestingly, the alkene content in the products was higher than 50 wt%. However, when Co-NPs were dispersed in polyethylene glycol (PEG) much lower activities were achieved (up to $0.12\,mol_{CO}\,mol_{Co}^{-1}\,h^{-1}$) than those obtained using the Fe-NPs.

Kou and co-workers also reported the use of Fe, Co and Ru NPs in F–T process in ethylene glycol (EG) and studied the formation of 2-alkyl-dioxolanes under syngas pressure at 130 °C [63b]. The highest selectivities to dioxolanes were achieved with Ru and Fe catalysts (up to 68% with Fe NPs) while the Co NPs mainly produced hydrocarbons (69%). The activities were in the order Ru ($1.5\,mol_{CO}\,mol_{Ru}^{-1}\,h^{-1}$) > Fe($0.68\,mol_{CO}\,mol_{Fe}^{-1}\,h^{-1}$) > Co($0.07\,mol_{CO}\,mol_{co}^{-1}\,h^{-1}$). The Fe catalyst exhibited a diameter of ca. 8 nm and was active with a range of other diols forming the corresponding acetals as the main products. Post-catalysis TEM studies of the Fe NPs revealed no relevant structural changes under catalytic conditions and these cheap catalysts could be easily recycled using a permanent magnet as they showed paramagnetic properties. The authors investigated into the mechanism of reaction and concluded that hydroformylation of syngas with olefins produced from F–T could be involved in the production of the dioxolanes.

7. Conclusions

Colloidal M-NPs have been applied in various catalytic processes and during the last decade, new methods for their synthesis and stabilisation have been reported. In this review, the current state of the art in the synthesis of soluble-Ru, Co and Fe-nanoparticles stabilised by organic molecules is described. Polymers are widely applied for the synthesis of soluble-Ru, Co and Fe-NPs, whereas the application of surfactants, ionic liquids and small molecules is much more limited.

The application of soluble-metal NPs as catalysts in the Fischer–Tropsch synthesis is of special interest as they provide high levels of activity and selectivity. The fine tuning of the M-NPs mean diameter and size dispersion and the choice of the stabilising agent and the solvent is of crucial importance in the design of more efficient catalytic systems. The successful application of soluble-metal nanocatalysts in the Fischer–Tropsch reaction using water, ionic liquids and high boiling point organic solvents was reported obtaining higher activities and selectivities than those obtained using the conventional supported catalysts. Several studies showed that water is a suitable solvent for the application of unsupported Ru-, Co- and Fe-NPs as catalysts in the Fischer–Tropsch reaction. In this solvent, the intra-particle transport of syngas and hydrocarbons is favoured enhancing the metal surface activity. Additionally, high C_5^+ selectivity with narrower product distributions were observed. Ru- and Co-NPs soluble in ionic liquids and Co and Fe-NPs soluble in high boiling point organic solvents, such as squalene and PEG, produced also interesting results in terms of Fischer–Tropsch catalytic performance.

Acknowledgments

The authors are grateful to Total S.A. (Gaz & Energies Nouvelles), the Spanish Ministerio de Educación y Ciencia (CTQ2007-62288/BQU, CTQ2010-14938/BQU, CTQ2008-01569-BQU, Consolider Ingenio 2010, and *Ramon y Cajal* fellowship to C. Godard) and the Generalitat de Catalunya (2009SGR116) for financial support.

References

[1] (a) G. Schmid, Clusters and Colloids From Theory to Applications, Wiley-VCH, Weinheim, 2004;
(b) G. Schmid, Nanoparticles, From Theory to Applications, Wiley-VCH, Weinheim, 1994.
[2] G.L. de Jongh, Physics and Chemistry of Metal Cluster Compounds, Kluwer, Dordrecht, 1994.
[3] K.J. Klabunde, G. Cardenas-Trivino, Active Metals: Preparation, Characterization, Applications, Wiley-VCH, Weinheim, 1996.
[4] L.N. Lewis, Catalysis by Di- and Polynuclear Metal Cluster, Wiley-VCH Inc., New York/Weinheim, 1998.
[5] D.L. Feldheim, C.A. Foss, Metal Nanoparticles, Marcel Dekker, New York, 2002.
[6] M.A. El-Sayed, Acc. Chem. Res. 34 (2001) 257.
[7] A. Roucoux, J. Schulz, H. Patin, Chem. Rev. 102 (2002) 3757.
[8] B.L. Cushing, V.L. Kolesnichenko, C.J. O'Connor, Chem. Rev. 104 (2004) 3893.
[9] E. Katz, I. Willner, Angew. Chem. Int. Ed. 43 (2004) 6042.
[10] K. Philippot, B. Chaudret, in: R.H. Crabtree, M.P. Mingos (Eds.), Comprehensive Organometallic Chemistry III, vol. 12, Elsevier, 2007, pp. 71–99 (Chapter 12.03).
[11] B. Chaudret, K. Philippot, Oil Gas Sci. Technol. 62 (2007) 799.
[12] (a) A. Müller, E. Beckmann, H. Bögge, M. Schmidtmann, A. Dress, Angew. Chem. Int. Ed. 41 (2002) 1162;
(b) V. Marvaud, C. Decroix, A. Scuiller, F. Tuyèras, C. Guyard-Duhayon, J. Vaissermann, J. Marrot, F. Gonnet, M. Verdaguer, Chem. Eur. J. 8 (2003) 1692.
[13] (a) H. Hirai, J. Macromol. Sci. Chem. 5 (1979) 633;
(b) W. Yu, M. Liu, H. Liu, X. Ma, Z. Liu, J. Colloid Interface Sci. 208 (1998) 439;
(c) M. Liu, M.W. Yu, H. Liu, J. Mol. Catal. A 138 (1999) 295;
(d) M.-P. Pileni, J. Phys. Chem. 97 (1993) 6961;
(e) K. Philippot, B. Chaudret, C.R. Chim. 6 (2003) 1019;
(f) M.-P. Pileni, Metal Nanoparticles, Marcel Dekker, New York, 2002.
[14] M.A. Vannice, J. Catal. 37 (1975) 449.
[15] (a) B. Jager, Stud. Surf. Sci. Catal. 119 (1998) 25;
(b) R.L. Espinoza, A.P. Steynberg, B. Jager, A.C. Vosloo, Appl. Catal. A 186 (1999) 13;
(c) B. Jager, R. Espinoza, Catal. Today 17 (1995) 23;
(d) M.E. Dry, Catal. Today 71 (2002) 227;
(e) T.C. Bromfield, A.C. Vosloo, Macromol. Symp. 193 (2003) 29.
[16] V. Balzani, Small 1 (2005) 278.
[17] B. Gates, Q. Xuo, M. Stewart, D. Ryan, G. Willson, G.M. Whitesides, Chem. Rev. 105 (2005) 1171.
[18] (a) J.D. Aiken III, R.G. Finke, J. Mol. Catal. A 145 (1999) 1;
(b) J.A. Widegren, R.G. Finke, J. Mol. Catal. A 191 (2003) 187.
[19] O. Vidoni, K. Philippot, C. Amiens, B. Chaudret, O. Balmes, J.O. Balm, F. Senocq, M.J. Casanove, Angew. Chem. Int. Ed. 38 (1999) 4.
[20] L. Starkey, R.G. Finke, Inorg. Chem. 45 (2006) 8382.
[21] H. Bönneman, G. Braun, W. Bnjoux, R. Brinkmann, A. Shculze Tilling, K. Seevogel, K. Siepen, J. Organomet. Chem. 520 (1996) 143.
[22] M. Green, Chem. Commun. (2005) 3002.
[23] J.P. Wilcoxon, B.L. Abrams, Chem. Soc. Rev. 35 (2006) 1162.
[24] B. He, Y. Ha, H. Liu, K. Wang, K.Y. Liew, J. Colloid Interface Sci. 308 (2007) 105.
[25] F. Lu, J. Liu, J. Xu, Mater. Chem. Phys. 108 (2008) 369.
[26] (a) F. Lu, J. Liu, J. Xu, Adv. Synth. Catal. 348 (2006) 857;
(b) F. Lu, J. Liu, J. Xu, J. Mol. Catal. A 271 (2007) 6.
[27] (a) C.X. Xiao, Z.P. Cai, T. Wang, Y. Kou, N. Yan, Angew. Chem. Int. Ed. 47 (2008) 746;
(b) Y. Kou, N. Yang, C. Xiao, Z. Cai, Y. Li, CA2681319, 2008.
[28] A. Gual, C. Godard, S. Castillón, C. Claver, in preparation.
[29] (a) M. Zawadzki, J. Okal, Mater. Res. Bull. 43 (2008) 3111;
(b) R. Harpness, Z. Peng, X.S. Liu, V.G. Pol, Y. Koltypin, A. Gedanken, J. Colloid Interface Sci. 287 (2005) 678;
(c) X. Yan, H. Liu, K.Y. Liew, J. Mater. Chem. 11 (2001) 3387;
(d) F. Bonet, V. Delmas, S. Grugeon, R. Herrera Urbina, P.Y. Silvert, K. Tekaia-Elhsissen, Nanostruct. Mater. 11 (1999) 1277;
(e) W. Tu, H. Liu, J. Mater. Chem. 10 (2007) 2207;
(f) F. Bensebaa, N. Patrito, Y. Le Page, P. L'Ecuyer, D. Wang, J. Mater. Chem. 14 (2004) 3378.

[30] (a) L.K. Kiruchara, G.M. Chow, P.E. Schoen, Nanostruct. Mater. 5 (1995) 607; (b) A. Miyazaki, K. Takeshita, K. Aika, Y. Nakano, Chem. Lett. 4 (1998) 361.
[31] M. Harada, S. Takahashi, J. Colloid Interface Sci. 325 (2008) 1.
[32] L. Song, X. Li, H. Wang, H. Wu, P. Wu, Catal. Lett. 133 (2009) 63.
[33] C.-W. Chen, C.-Y. Chen, Y.-H. Huang, Int. J. Hydrogen Energy 34 (2009) 2164.
[34] R.A. Sánchez-Delgado, N. Machalaba, N. Ng-a-qui, Catal. Commun. 8 (2007) 2115.
[35] J. Ma, H. Ma, D. Pan, R. Li, K. Xie, React. Kinet. Catal. Lett. 86 (2005) 225.
[36] (a) G. Lafaye, C.T. Williams, M.D. Amiridis, Catal. Lett. 96 (2004) 43; (b) G. Lafaye, A. Siani, P. Marécot, M.D. Amiridis, C.T. Williams, J. Phys. Chem. B 110 (2006) 7725.
[37] X. Zhou, T. Wu, B. Hu, T. Jiang, B. Han, J. Mol. Catal. A 306 (2009) 143.
[38] A. Duteil, R. Queau, B. Chaudret, Chem. Mater. 5 (1993) 341.
[39] J. Osuna, D. Caro, C. Amiens, B. Chaudret, E. Snoeck, M. Respaud, J.M. Broto, A. Fert, J. Phys. Chem. 100 (1996) 14571.
[40] C. Pan, K. Pelzer, K. Philippot, B.B. Chaudret, F. Dassenoy, P. Lecante, M.J. Casanove, J. Am. Chem. Soc. 123 (2001) 7584.
[41] F. Novio, K. Philippot, B. Chaudret, Catal. Lett. 104 (2010) 1.
[42] N. Mejías, A. Serra-Muns, R. Pleixats, A. Shafir, M. Tristany, Dalton Trans. (2009) 7748.
[43] D. Wostek-Wojciechowska, J.K. Jeszka, C. Amiens, B. Chaudret, P. Lecante, J. Colloid Interface Sci. 287 (2005) 107.
[44] (a) T.Q. Hu, B.R. James, J.S. Retting, C. Lee, Can. J. Chem. 75 (1997) 1234; (b) T.Q. Hu, B.R. James, C. Lee, J. Pulp Paper Sci. 23 (1997) J153; (c) B.R. James, Y. Wang, C.S. Alexander, T.Q. Hu, Chem. Ind. 750 (1998) 233.
[45] (a) J. Schulz, A. Roucoux, H. Patin, Chem. Eur. J. 6 (2000) 618; (b) J. Schulz, S. Levigne, A. Roucoux, H. Patin, Adv. Synth. Catal. 344 (2002) 266; (c) A. Roucoux, J. Schulz, H. Patin, Adv. Synth. Catal. 345 (2003) 222; (d) V. Mévellec, A. Roucoux, E. Ramirez, K. Phillipot, B. Chaudret, Adv. Synth. Catal. 346 (2004) 72; (e) A. Nowicki, V. Le Boulaire, A. Roucoux, Adv. Synth. Catal. 349 (2007) 2326; (f) C. Hubert, A. Denicourt-Nowicki, J.P. Guégan, A. Roucoux, Dalton Trans. (2009) 7356; (g) V. Mévellec, A. Nowicki, A. Roucoux, C. Dujardin, P. Granger, E. Payen, K. Philippot, New J. Chem. 30 (2006) 1214; (h) L. Barthe, M. Hemati, K. Phillipot, B. Chaudret, A. Denicourt-Nowicki, A. Roucoux, Chem. Eng. J. 151 (2009) 372.
[46] C. Hubert, A. Denicourt-Nowicki, A. Roucoux, D. Landy, B. Leger, G. Crowyn, E. Monflier, Chem. Commun. (2009) 1228.
[47] J. Dupont, G.S. Fonseca, A.P. Umpierre, P.F.P. Fichtner, S.R. Teixeira, J. Am. Chem. Soc. 124 (2002) 4228.
[48] (a) T. Gutel, J. Garcia-Anton, K. Pelzer, K. Philippot, C. Santini, Y. Chauvin, B. Chaudret, J.M. Basset, J. Mater. Chem. 17 (2007) 3290; (b) P. Migowski, G. Machado, S.R. Texeira, M.C.M. Alves, J. Morais, A. Traverse, J. Dupont, Phys. Chem. Chem. Phys. 9 (2007) 4814; (c) E. Redel, R. Thomann, C. Janiak, Inorg. Chem. 47 (2008) 14; (d) E. Redel, R. Thomann, C. Janiak, Chem. Commun. (2008) 1789.
[49] (a) J.D. Scholten, G. Ebeling, J. Dupont, Dalton Trans. (2007) 5554; (b) C.W. Scheeren, G. Machado, S.R. Teixeira, J. Morais, J.B. Domingos, J. Dupont, J. Phys. Chem. B 110 (2006) 13011; (c) G.S. Fonseca, G. Machado, S.R. Teixeira, G.H. Fecher, J. Morais, M.C.M. Alves, J. Dupont, J. Colloid Interface Sci. 301 (2006) 193.
[50] E.T. Silveira, A.P. Umpierre, L.M. Rossi, G. Machado, J. Morais, G.V. Soares, I.L.R. Baumvol, S.R. Teixeira, P.F.P. Fichtner, J. Dupont, Chem. Eur. J. 10 (2004) 3734.
[51] (a) P.S. Campbell, C.C. Santini, D. Bouchu, B. Fenet, K. Philippot, B. Chaudret, A.A.H. Pádua, Y. Chauvin, Phys. Chem. Chem. Phys. 12 (2010) 4217; (b) P.S. Campbell, C.C. Santini, F. Bayard, Y. Chauvin, V. Collière, A. Podgoršek, M.F. Costa Gomes, J. Sá, J. Catal. 275 (2010) 99.
[52] (a) M.H.G. Prechtl, M. Scariot, J.D. Scholten, G. Machado, S.R. Teixeira, J. Dupont, Inorg. Chem. 47 (2008) 8995; (b) M.H.G. Prechtl, J.D. Scholten, J. Dupont, J. Mol. Catal. A 313 (2009) 74.
[53] (a) L.M. Rossi, G. Machado, J. Mol. Catal. A 298 (2009) 69; (b) L.M. Rossi, G. Machado, P.F.P. Fichtner, S.R. Teixeira, J. Dupont, Catal. Lett. 92 (2004) 149.
[54] C. Vollmer, E. Redel, K. Abu-Shandi, R. Thomann, H. Manyar, C. Hardacre, C. Janiak, Chem. Eur. J. 16 (2010) 3849.
[55] J. Huang, T. Jiang, B. Han, W. Wu, Z. Liu, Z. Xie, J. Zhang, Catal. Lett. 103 (2005) 1.
[56] S. Miao, Z. Liu, B. Han, J. Huang, Z. Sun, J. Zhang, T. Jiang, Angew. Chem. Int. Ed. 45 (2006) 266.
[57] F. Xiao, F. Zhao, D. Mei, Z. Mo, B. Zeng, Biosens. Bioelectron. 24 (2009) 3481.
[58] A. Gual, C. Godard, S. Castillón, C. Claver, Dalton Trans. 39 (2010) 11499.
[59] M.V. Escárcega-Bobadilla, C. Tortosa, E. Teuma, C. Pradel, A. Orejón, M. Gómez, A.M. Masdeu-Bultó, Catal. Today 148 (2009) 398.
[60] J. García-Antón, M.R. Axet, S. Jansat, K. Philippot, B. Chaudret, T. Pery, G. Buntkowsky, H.H. Limbach, Angew. Chem. Int. Ed. 47 (2008) 2074.
[61] (a) A. Gual, M.R. Axet, K. Philippot, B. Chaudret, A. Denicourt-Nowicki, A. Roucoux, S. Castillón, C. Claver, Chem. Commun. (2008) 2759; (b) A. Gual, C. Godard, K. Philippot, B. Chaudret, A. Denicourt-Nowicki, A. Roucoux, S. Castillón, C. Claver, ChemSusChem 2 (2009) 769.
[62] O. Metin, S. Özkar, Energy Fuel 23 (2009) 3517.
[63] (a) X.-B. Fan, Z.-Y. Tao, C.-X. Xiao, F. Liu, Y. Kou, Green Chem. 12 (2010) 795; (b) X.-B. Fan, N. Yan, Z.-Y. Tao, D. Evans, C.-X. Xiao, Y. Kou, ChemSusChem 2 (2009) 941.
[64] N. Yan, J.-g. Zhang, Y. Tong, S. Yao, C. Xiao, Z. Li, Y. Kou, Chem. Commun. (2009) 4423.
[65] L.T. Lu, L.D. Tung, I. Robinson, D. Ung, B. Tan, J. Long, A.I. Cooper, D.G. Fernigde, N.T.K. Thanh, J. Mater. Chem. 18 (2008) 2453.
[66] I.-W. Park, M. Yoon, Y.M. Kim, Y. Kim, J.H. Kim, S. Kim, V. Volkov, J. Magn. Magn. Mater. 272–276 (2004) 1413.
[67] K. Pirkkalainen, K. Leppänen, U. Vainio, M.A. Webb, T. Elbra, T. Kohout, A. Nykänen, J. Ruokolainen, N. Kotelnikova, R. Serimaa, Eur. Phys. J. D 49 (2008) 333.
[68] I. Robinson, C. Alexander, L.T. Lu, L.D. Tung, D.G. Fernig, N.T.K. Thanh, Chem. Commun. (2007) 4602.
[69] (a) M.M. Bull, W.J. Chung, S.R. Anderson, S.-J. Kim, I.-B. Shim, H.-J. Paik, J. Pyun, J. Mater. Chem. 20 (2010) 6023; (b) P.Y. Keng, I. Shim, B.D. Korth, J.F. Douglas, J. Pyun, ACS Nano 1 (2007) 279.
[70] O.A. Platonova, L.M. Bronstein, S.P. Solodovnikov, I.M. Yanovskaya, E.S. Obolonkova, P.M. Valetsky, E. Wenz, M. Antonietti, Colloid Polym. Sci. 275 (1997) 426.
[71] F.S. Diana, S.-H. Lee, P.M. Petroff, E.J. Kramer, Nano Lett. 7 (2003) 891.
[72] E.H. Tadd, J. Bradley, R. Tannenbaum, Langmuir 18 (2002) 2378.
[73] M. Rutnakornpituk, M.S. Thompson, L.A. Harris, K.E. Farmer, A.R. Esker, J.S. Riffle, J. Conolly, T.G. St. Pierre, Polymer 43 (2002) 2337.
[74] R. Qiao, X.L. Zhang, R. Qiu, Y. Li, Y.S. Kang, J. Phys. Chem. C 111 (2007) 2426.
[75] L. Zadoina, K. Soulantica, S. Ferrere, B. Lonetti, M. Respaud, A.-F. Mingotaud, A. Falqui, A. Genovese, B. Chaudret, M. Mauzac, J. Mater. Chem. 21 (2011) 6988.
[76] H. Ago, T. Komatsu, S. Ohshima, Y. Kuriki, M. Yumura, Appl. Phys. Lett. 77 (2000) 79.
[77] N.D. Subramanian, G. Balaji, C.S.S.R. Kumar, J.J. Spivey, Catal. Today 147 (2009) 100.
[78] (a) C. Petit, A. Taleb, M.-P. Pileni, Adv. Mater. 10 (1998) 259; (b) C. Petit, M.-P. Pileni, J. Magn. Magn. Mater. 166 (1997) 82.
[79] C.C. Cassol, G. Ebeling, B. Ferrera, J. Dupont, Adv. Synth. Catal. 348 (2006) 243.
[80] D.O. Silva, J.D. Scholten, M.A. Gelesky, S.R. Teixeira, A.C.B. Dos Santos, E.F. Souza-Aguiar, J. Dupont, ChemSusChem 1 (2008) 291.
[81] M. Scariot, D.O. Silva, J.D. Scholten, G. Machado, S.R. Teixeira, M.A. Novak, G. Ebeling, J. Dupont, Angew. Chem. Int. Ed. 47 (2008) 9075.
[82] G. Machado, J.D. Scholten, T. de Vargas, S.R. Teixeira, L.H. Ronchi, J. Dupont, Int. J. Nanotechnol. 4 (2007) 541.
[83] S. Sun, C.B. Murray, J. Appl. Phys. 85 (1999) 4325.
[84] (a) H.T. Yang, Y.K. Su, C.M. Shen, T.Z. Yang, H.J. Gao, Surf. Interface Anal. 36 (2004) 155; (b) Y. Bao, B. Pakhomov, K.M. Krishnan, J. Appl. Phys. 97 (2005) 10J317; (c) D.P. Dinega, M.G. Bawendi, Angew. Chem. Int. Ed. 38 (1999) 1788.
[85] Y. Su, X.O. Yang, J. Tang, Appl. Surf. Sci. 256 (2010) 2353.
[86] N. Wu, L. Fu, M. Su, M. Aslam, K.C. Wong, V.P. Dravid, Nano Lett. 4 (2004) 383.
[87] V.F. Puntes, K.M. Krishnan, P. Alivisatos, Science 291 (2001) 2115.
[88] J. Schällibaum, F.H. Dalla Torre, W.R. Caseri, J.F. Löffler, Nanoscale 1 (2009) 374.
[89] A. Samia, K. Hyzer, J. Schlueter, C.-J. Qin, S. Jiang, S. Bader, X.-M. Lin, J. Am. Chem. Soc. 127 (2005) 4126.
[90] (a) F. Dumestre, B. Chaudret, C. Amiens, M.-C. Fromen, M.-J. Casanove, P. Renaud, P. Zurcher, Angew. Chem. Int. Ed. 41 (2002) 4286; (b) F. Dumestre, B. Chaudret, C. Amiens, M. Respaud, P. Fejes, P. Renaud, P. Zurcher, Angew. Chem. Int. Ed. 42 (2003) 5213; (c) E. Snoeck, R.E. Dunin-Borkowski, F. Dumestre, P. Renaud, C. Amiens, B. Chaudret, P. Zurcher, Appl. Phys. Lett. 82 (2003) 88.
[91] F. Wetz, K. Soulantica, M. Respaud, A. Falqui, B. Chaudret, Mater. Sci. Eng. C 27 (2007) 1162.
[92] K.-C. Huang, S.H. Ehrman, Langmuir 23 (2007) 1419.
[93] S. Xiao, M. Shen, R. Guo, S. Wang, X. Shi, J. Phys. Chem. C 113 (2009) 18062.
[94] (a) S. Xiao, H. Ma, M. Shen, S. Wang, Q. Huang, X. Shi, Coll. Surf. A 381 (2011) 48; (b) S. Xiao, M. Shen, R. Guo, Q. Huang, S. Wang, X. Shi, J. Mater. Chem. 20 (2010) 5700.
[95] Y.-P. Sun, X.-Q. Li, W.-X. Zhang, H.P. Wang, Colloid Surf. A 308 (2007) 60.
[96] F. He, M. Zhang, T. Qian, D. Zhao, J. Colloid Interface Sci. 334 (2009) 96.
[97] J. Fatisson, S. Ghoshal, N. Tufenkji, Langmuir 26 (2010) 12832.
[98] S.M. Ponder, J.G. Darab, J. Bucher, D. Caulder, I. Craig, L. Davis, N. Edelstein, W. Lukens, H. Nitsche, L. Rao, D.K. Shuh, T.E. Mallouk, Chem. Mater. 13 (2001) 479.
[99] K.S. Suslick, M. Fang, T. Hyeon, J. Am. Chem. Soc. 118 (1996) 11960.
[100] H. Khalil, D. Mahajan, M. Rafailovich, M. Gelfer, K. Pandya, Langmuir 20 (2004) 6896.
[101] N.A.D. Burke, H.D.H. Stöver, F.P. Dawson, Chem. Mater. 14 (2002) 4752.
[102] O. Margeat, F. Dumestre, C. Amiens, B. Chaudret, P. Lecante, M. Respaud, Prog. Solid State Chem. 33 (2005) 71.
[103] J.P. Wilcoxon, P.P. Provencio, J. Phys. Chem. B 103 (1999) 9809.
[104] J. Krämer, E. Redel, R. Thomann, C. Janiak, Organometallics 27 (2008) 1976.
[105] L. Lartigue, R. Pflieger, S.I. Nikitenko, Y. Guari, L. Stievano, M.T. Sougrati, J. Larionova, Phys. Chem. Chem. Phys. 13 (2011) 2111.
[106] Y.-L. Zhu, Y. Katayama, T. Miura, ECS Trans. 32 (2010) 537.
[107] X. Cheng, B. Wu, Y. Yang, H. Xiang, Y. Li, J. Mol. Catal. A 329 (2010) 103.
[108] G.E. Hoag, J.B. Collins, J.L. Holcomb, J.R. Hoag, M.N. Nadagouda, R.S. Varma, J. Mater. Chem. 19 (2009) 8671.
[109] R.B. Bedford, M. Betham, D.W. Bruce, S.A. Davis, R.M. Frost, M. Hird, Chem. Commun. (2006) 1398.

[110] C. Rangheard, C. de Julián-Fernández, P.-H. Phua, J. Hoorn, L. Lefort, J.G. de Vries, Dalton Trans. 39 (2010) 8464.
[111] P.-H. Phua, L. Lefort, J.A.F. Boogers, M. Tristany, J.G. de Vries, Chem. Commun. (2009) 3747.
[112] S.-J. Park, S. Kim, S. Lee, Z.G. Khim, K. Char, T. Hyeon, J. Am. Chem. Soc. 122 (2000) 8581.
[113] T. Hyeon, S. Lee, J. Park, Y. Chung, H.B. Na, J. Am. Chem. Soc. 123 (2001) 12798.
[114] L. Guo, Q. Huang, X.-Y. Li, S. Yang, Phys. Chem. Chem. Phys. 3 (2001) 1661.
[115] M. Maeda, C.S. Kuroda, T. Shimura, M. Tada, M. Abe, S. Yamamuro, K. Sumiyama, H. Handa, J. Appl. Phys. 99 (2006) 08H103.
[116] F. Dumestre, B. Chaudret, C. Amiens, P. Renaud, P. Fejes, Science 303 (2004) 821.
[117] (a) A.P. Steynberg, M.E. Dry, Fischer–Tropsch Technology, Elsevier, Amsterdam, 2004;
(b) B.H. Davis, M.L. Occelli, Fischer–Tropsch Synthesis, Catalysts and Catalysis, Amsterdam, 2007.
[118] (a) P.B. Anderson, The Fischer–Tropsch Synthesis, Academic Press, London, 1984;
(b) M. Röper, Catalysis in C1 Chemistry, D. Reidel, Dordrecht, 1983;
(c) A.A. Adesina, Appl. Catal. A 138 (1986) 345;
(d) Y.T. Shah, A.J. Perrota, Ind. Eng. Chem. Prod. Res. Dev. 15 (1976) 123.
[119] J. Kang, S. Zhang, Q. Zhang, Y. Wang, Angew. Chem. Int. Ed. 48 (2009) 2565.
[120] S. Zhao, V.S. Nagineni, N.V. Seetala, D. Kuila, Ind. Eng. Chem. Res. 47 (2008) 1684.
[121] M. Claeys, E. van Steen, Catal. Today 71 (2002) 419.
[122] M.L. Turner, N. Marsih, B.E. Mann, R. Quyoum, H.C. Long, P.M. Maitlis, J. Am. Chem. Soc. 124 (2002) 10456.
[123] (a) S.H. Song, S.B. Lee, J.W. Bae, S. Prasad, K.W. Jun, Y.G. Shul, Catal. Lett. 129 (2009) 233;
(b) L. Guillou, S. Paul, V. Le Courtois, Chem. Eng. J. 136 (2008) 66;
(c) G. Kiss, C.E. Kliewer, G.J. DeMartin, C.C. Culross, J.E. Baumgartner, J. Catal. 217 (2003) 127;
(d) J. Shen, E. Schmetz, G.J. Kawalkin, G.J. Stiegel, R.P. Noceti, J.C. Winslow, R.M. Kornosky, D. Krastman, V.K. Venkataraman, D.J. Driscoll, D.C. Cicero, W.F. Haslebacher, B.C.B. Hsieh, S.C. Jain, J.B. Tennant, Top. Catal. 26 (2003) 13;
(e) S.L. Soled, E. Iglesia, R.A. Fiato, J.E. Baumgartner, H. Vroman, S. Miseo, Top. Catal. 26 (2003) 101;
(f) J.G. Chen, H.W. Xiang, H.Y. Gao, Y.H. Sun, React. Kinet. Mech. Catal. 73 (2001) 169;
(g) S. Yan, L. Fan, Z. Zhanga, J. Zhoua, K. Fujimoto, Appl. Catal. A 171 (1998) 247.
[124] A.K. Dalai, B.H. Davis, Appl. Catal. A 348 (2008) 1.
[125] A. Manivannan, N. Elbashir, P. Dutta, C.B. Roberts, M. Seehra, Appl. Catal. A 285 (2005) 169.
[126] X. Li, M. Luo, K. Asami, Catal. Today 89 (2004) 439.
[127] X. Liu, W. Linghu, X. Li, K. Asami, K. Fujimoto, Appl. Catal. A 303 (2006) 251.
[128] A.Y. Khodakov, R. Bechara, A. Griboval-Constant, Appl. Catal. A 254 (2003) 273.
[129] (a) N. Lohitharn, J.G. Goodwinjr, J. Catal. 257 (2008) 142;
(b) N. Lohitharn, J.G. Goodwinjr, J. Catal. 260 (2008) 7;
(c) N. Lohitharn, J.G. Goodwinjr, E. Lotero, J. Catal. 255 (2008) 104;
(d) J. Xu, C.H. Bartholomew, J. Sudweeks, D.L. Eggett, Top. Catal. 26 (2003) 55;
(e) G.P. van der Laan, A.A.C.M. Beenackers, Appl. Catal. A 193 (2000) 39.
[130] D.B. Bukur, C. Sivaraj, Appl. Catal. A 231 (2002) 201.
[131] R.J. O'Brien, L. Su, R.L. Spicer, B.H. Davis, Energy Fuels 10 (1996) 221.
[132] T. Riedel, H. Schulz, G. Schaub, K.W. Jun, J.S. Hwang, K.W. Lee, Top. Catal. 26 (2003) 145.
[133] (a) A. Irankhah, A. Haghtalab, Chem. Eng. Technol. 31 (2008) 525;
(b) V. Ragaini, R. Carli, C.L. Bianchi, D. Lorenzetti, G. Predieri, P. Moggi, Appl. Catal. A 139 (1996) 31.
[134] (a) S. Lögdberg, D. Tristantini, Ø. Borg, L. Ilver, B. Gevert, S. Järås, E.A. Blekkan, A. Holmen, Appl. Catal. B 89 (2009) 167;
(b) D.J. Moodley, A.M. Saib, M.J. Overett, A.K. Datye, J.W. Niemantsverdriet, Appl. Catal. A 354 (2009) 102;
(c) A. Tavasoli, R.M.M. Abbaslou, M. Trépanier, A.K. Dalai, Appl. Catal. A 345 (2008) 134;
(d) D. Tristantini, A. Holmen, Fuel Proces. Technol. 88 (2007) 643;
(e) X. Huang, N.O. Elbashir, C.B. Roberts, Ind. Eng. Chem. Res. 43 (2004) 6369;
(f) X. Huang, C.B. Roberts, Fuel Process. Technol. 83 (2003) 81;
(g) R. Bechara, D. Balloy, D. Vanhove, Appl. Catal. A 207 (2001) 343;
(h) A.-M. Hilmen, E. Bergene, D. Schanke, S. Eri, A. Holmen, Catal. Today 69 (2001) 227;
(i) A.N. Akin, Z.I. Onsan, J. Chem. Technol. Biotechnol. 70 (1997) 304.
[135] C. Pirola, C.L. Bianchi, A.D. Michele, S. Vitali, V. Ragaini, Catal. Commun. 10 (2009) 823.
[136] H.J. Wan, B.S. Wu, C.H. Zhang, H.W. Xiang, Y.W. Li, B.F. Xu, F. Yi, Catal. Commun. 8 (2007) 1538.
[137] D.A. Simonetti, J. Rass-Hansen, E.L. Kunkes, R.R. Soares, J.A. Dumesic, Green Chem. 9 (2007) 1073.
[138] (a) C.J. Bertole, C.A. Mims, G. Kiss, J. Catal. 96 (2002) 84;
(b) K. Jothimurugesan, S.K. Gangwal, Ind. Eng. Chem. Res. 37 (1998) 1181.
[139] A. Tavasoli, M. Trépanier, R.M. Malek Abbaslou, A.K. Dalai Abatzoglou, Fuel Process. Technol. 90 (2009) 1486.
[140] E. van Steen, F.F. Prinsloo, Catal. Today 71 (2002) 327.
[141] (a) D.Y. Murzin, Chem. Eng. Sci. 64 (2009) 1046;
(b) G.L. Bezemer, J.H. Bitter, H.P.C.E. Kuipers, H. Oosterbeek, J.E. Holewijn, X. Xu, F. Kapteijn, A.J. van Dillen, K.P. de Jong, J. Am. Chem. Soc. 128 (2006) 3956.
[142] W. Ma, E.L. Kugler, Dadyburjor, Energy Fuel. 21 (2007) 1832.
[143] Y.A. Taran, G.A. Kliger, V.S. Sevastianov, Geochim. Cosmochim. Acta 71 (2007) 4474.
[144] G. Prieto, A. Martinez, P. Concepcion, R. Moreno-Tost, J. Catal. 266 (2009) 129.
[145] P. Wasserscheid, W. Keim, Angew. Chem. Int. Ed. 39 (2000) 3772.
[146] M.D. Shroff, D.S. Kalakkad, K.E. Coulter, S.D. Koehler, M.S. Harrington, N.B. Jackson, A.G. Sault, A.K. Datye, J. Catal. 156 (1995) 185.
[147] C.J. Weststrate, A. Resta, R. Westerström, E. Lundgren, A. Mikkelsen, J.N. Andersen, J. Phys. Chem. C 112 (2008) 6900.
[148] (a) B. Hammer, J.K. Nørskov, Adv. Catal. 45 (2000) 71;
(b) J.K. Nørskov, T. Bligaard, A. Logadottir, S. Bahn, L.B. Hansen, M. Bollinger, H.S. Bengaard, B. Hammer, Z. Sljivancanin, M. Mavrikakis, Y. Xu, S. Dahl, C.J.H. Jacobsen, J. Catal. 209 (2002) 275.
[149] C.P. Vinod, Catal. Today 154 (2010) 113.
[150] E. Iglesia, Appl. Catal. A 161 (1997) 59.
[151] (a) R.C. Reuel, C.H. Bartholomew, J. Catal. 85 (1984) 78;
(b) H. Schulz, E. Van Steen, M. Claeys, Stud. Surf. Sci. Catal. 81 (1994) 204.
[152] (a) M.E. Dry, in: J.R. Anderson, M. Boudart (Eds.), Catalysis Science and Technology, vol. 1, Springer-Verlag, Berlin, 1981, pp. 195–300;
(b) B.H. Davis, Fuel Process. Technol. 71 (2001) 157;
(c) J. Ming, N. Koizumi, T. Ozaki, M. Yamada, Appl. Catal. A 209 (2001) 59;
(d) G. Bian, N. Fujishita, T. Mochizuki, W. Ning, M. Yamada, Appl. Catal. A 252 (2003) 251;
(e) G. Bian, T. Mochizuki, N. Fujishita, H. Nomoto, M. Yamada, Energy Fuels 17 (2003) 799;
(f) S. Sun, N. Tsubaki, K. Fujimoto, Appl. Catal. A: Gen. 202 (2000) 121;
(g) A. Feller, M. Claeys, E. van Steen, J. Catal. 185 (1999) 120;
(h) G. Prieto, A. Martinez, P. Concepcion, R. Moreno-Tost, J. Catal 266 (2009) 129.
[153] (a) M. Shinoda, Y. Zhang, Y. Yomeyama, K. Hasegawa, N. Tsubaki, Fuel Proc. Technol. 86 (2004) 73;
(b) Y. Zhang, M. Koike, R. Yang, S. Hinchiranan, T. Vitidsant, N. Tsubaki, Appl. Catal. A: Gen. 292 (2005) 252.
[154] (a) G. Jacobs, J.A. Chaney, P.M. Patterson, T.K. Das, B.H. Davis, Appl. Catal. A: Gen. 264 (2004) 203;
(b) G. Jacobs, P.M. Patterson, T.K. Das, B.H. Davis, Appl. Catal. A: Gen. 270 (2004) 65.
[155] J.P. den Breejen, J.R.A. Sietsma, H. Friedrich, J.H. Bitter, K.P. de Jong, J. Catal. 270 (2010) 146.
[156] (a) A.Y. Khodakov, J. Lynch, D. Bazin, B. Rebours, N. Zanier, B. Moisson, P. Chaumette, J. Catal. 168 (1997) 16;
(b) A. Martinez, C. Lopez, F. Marquez, I. Diaz, J. Catal. 220 (2003) 486;
(c) A. Kogelbauer, J.C. Weber, J.G. Goodwin, Catal. Lett. 34 (1995) 259;
(d) P.J. van Berge, J. van de Loosdrecht, S. Barradas, A.M. van der Kraan, Catal. Today 58 (2000) 321;
(e) Y. Zhang, D. Wei, S. Hammache, J.G. Goodwin, J. Catal. 188 (1999) 281.
[157] A.M. Saib, A. Borgna, J. van de Loosdrecht, P.J. van Berge, J.W. Niemantsverdriet, Appl. Catal. A 312 (2006) 12.
[158] (a) A. Navrotsky, C. Ma, K. Lilova, N. Birkner, Science 330 (2010) 199;
(b) E. van Steen, M. Claeys, M.E. Dry, J. van de Loosdrecht, E.L. Viljoen, J.L. Visagie, J. Phys. Chem. B 109 (2005) 3575.
[159] (a) A.N. Pour, M.R. Housaindokht, S.F. Tayyari, J. Zarkesh, J. Nat. Gas Chem. 19 (2010) 107;
(b) A.N. Pour, S. Taghipoor, M. Shekarriz, S.M.K. Shahri, Y. Zamani, J. Nanosci, Nanotechnology 9 (2009) 4425;
(c) A. Sarkar, D. Seth, A.K. Dozier, J.K. Neathery, H.H. Hamdeh, B.H. Davis, Catal. Lett. 117 (2007) 1;
(d) T. Herranz, S. Rojas, F.J. Perez-Alonso, M. Ojeda, P. Terreros, J.L.G. Fierro, Appl. Catal. A 311 (2006) 66;
(e) S. Eriksson, U. Nylen, S. Rojas, M. Boutonnet, Appl. Catal. A 265 (2004) 207.
[160] N. Yan, C. Xiao, Y. Kou, Coord. Chem. Rev. 254 (2010) 1179.
[161] C.J. Kim, US5227407 (A) (1993), to Exxon Research and Engineering Company.
[162] H.F. Klein, Appl. Catal. A 350 (2008) 126.
[163] (a) S. Krishnamoorthy, M. Tu, M.P. Ojeda, D. Pinna, E. Iglesia, J. Catal. 211 (2002) 422;
(b) C.J. Bertole, C.A. Mims, G. Kiss, J. Catal. 210 (2002) 84;
(c) E. van Steen, H. Schulz, Appl. Catal. A 186 (1999) 309;
(d) T.K. Das, W.A. Conner, J. Li, G. Jacobs, M.E. Dry, B.H. Davis, Energy Fuels 19 (2005) 1430.
[164] A.K. Dalai, T.K. Das, K.V. Chaudhari, G. Jacobs, B.H. Davis, Appl. Catal. A 289 (2005) 135.
[165] (a) I.C. Yates, C.N. Satterfield, Energy Fuels 5 (1991) 168;
(b) A.O.I. Rautavuoma, S. van der Baan, Appl. Catal. 1 (1981) 247;
(c) B. Sarup, B.W. Wojciechowski, Can. J. Chem. Eng. 67 (1989) 62;
(d) G.P. van der Laan, A.A.C.M. Beenackers, Catal. Rev.-Sci. Eng. 41 (1999) 255.
[166] E.A. Blekkan, Ø. Borg, V. Frøseth, A. Holmen, Catalysis, vol. 20, Royal Society of Chemistry, 2007.
[167] (a) Ø. Borg, S. Storsæter, S. Eri, H. Wigum, E. Rytter, A. Holmen, Catal. Lett. 107 (2006) 95;
(b) S. Storsæter, Ø. Borg, E.A. Blekkan, A. Holmen, J. Catal. 231 (2005) 405;
(c) D. Schanke, A.M. Hilmen, E. Bergene, K. Kinnari, E. Rytter, E. Ådnanes, A. Holmen, Energy Fuels 10 (1996) 867;

(d) A.M. Hilmen, O.A. Lindvåg, E. Bergene, D. Schanke, S. Eri, A. Holmen, Stud. Surf. Sci. Catal. 136 (2001) 295;
(e) J. Li, X. Zhan, Y. Zhang, G. Jacobs, T. Das, B.H. Davis, Appl. Catal. A 228 (2002) 203;
(f) S. Lögdberg, M. Boutonnet, J.C. Walmsley, S. Järås, A. Holmen, E.A. Blekkan, Appl. Catal. A 393 (2011) 109.
[168] (a) D. Schanke, A.M. Hilmen, E. Bergene, K. Kinnari, E. Rytter, E. Ådnanes, A. Holmen, Catal. Lett. 34 (1995) 269;
(b) A.M. Hilmen, D. Schanke, K.F. Hanssen, A. Holmen, Appl. Catal. A 186 (1999) 169;
(c) K.F. Hanssen, E.A. Blekkan, D. Schanke, A. Holmen, Stud. Surf. Sci. Catal. 109 (1997) 193.
[169] S. Eri, K.J. Kinnari, D. Schanke, A.M. Hilmen, WO0247816 (A1) (2002), to Statoil ASA.
[170] G. Jacobs, T.K. Das, P.M. Patterson, J. Li, L. Sanchez, B.H. Davis, Appl. Catal. A 247 (2003) 335.
[171] (a) J. Li, G. Jacobs, T. Das, Y. Zhang, B. Davis, Appl. Catal. A 236 (2002) 67;
(b) H. Schulz, E. van Steen, M. Claeys, Stud. Surf. Sci. Catal. 81 (1994) 455.
[172] C.J. Kim, EP0339923 (B1) (1994), to Exxon Research and Engineering Company.
[173] J. Li, G. Jacobs, T. Das, B.H. Davis, Appl. Catal. A 233 (2002) 255.
[174] (a) Y. Li, Y. Fan, H. Yang, B. Xu, L. Feng, M. Yang, Y. Chen, Chem. Phys. Lett. 372 (2003) 160;
(b) G.L. Haller, D.E. Resasco, Adv. Catal. 36 (1989) 173.
[175] (a) G. Jacobs, Y. Zhang, T.K. Das, J. Li, P.M. Patterson, B.H. Davis, Stud. Surf. Sci. Catal. 139 (2001) 415;
(b) G. Jacobs, P.M. Patterson, Y. Zhang, T. Das, J. Li, B.H. Davis, Appl. Catal. A 233 (2002) 215;
(c) J. van de Loosdrecht, B. Balzhinimaev, J.A. Dalmon, J.W. Niemantsverdriet, S.V. Tsybulya, A.M. Saib, P.J. van Berge, J.L. Visagie, Catal. Today 123 (2007) 293.
[176] C.H. Bartholomew, Appl. Catal. A 212 (2001) 17.